were injected intravenously into each type of mice. Immunological assays were performed 2 weeks after injection.

### Confirmation of pDC depletion in spleen by flow cytometric analysis

After Fc blocking with an antibody to CD16/32, isolated spleen cells were stained with fluorescein isothiocyanate (FITC)–conjugated antibody to CD11c, phycoerythrin (PE)–conjugated antibody to CD45R/B220, and allophycocyanin-conjugated antibody to mPDCA-1 (Miltenyi Biotec) for 30 min at room temperature and washed with PBS containing 1% bovine serum albumin. Just before fluorescence-activated cell sorting (FACS) analysis using FACSCalibur and CellQuest software (BD Biosciences), 7-aminoactinomycin D (BD Biosciences) was added.

### Measurement of antigen-specific T and B cell responses

After two i.n. vaccinations, B cell–mediated humoral responses were measured as immunoglobulin production by ELISA using goat antibody to mouse total IgG, IgG1, IgG2a, and IgA conjugated to horseradish peroxidase (Southern Biotech) as previously described (*1*). T cell–mediated cellular responses were monitored by measuring $NP_{260–283}$/I-$A^b$–specific or $NP_{366–374}$/H-$2D^b$–specific IFN-γ secretion of splenocytes and the frequency and cytotoxicity of H-$2D^b$–specific CD8 T cells as described previously (*13*).

### Preparation of human PBMCs for cytokine analysis

PBMCs were obtained from 10 healthy adult volunteers (30 to 50 years old, 6 males and 4 females). All of the experiments using human PBMCs were approved by the Institutional Review Board of the Research Institute for Microbial Diseases, Osaka University. Cells were purified from heparinized blood by density centrifugation using Ficoll-Paque Plus (Amersham). Human pDCs, CD4, or CD8 T cells were depleted with BDCA4 and CD4 or CD8 antibody MACS microbeads (Miltenyi Biotec), respectively, according to the manufacturer's protocol. Plasmacytoid DC depletion was confirmed by FACS analysis staining with FITC-conjugated antibody to BDCA2 and PE-conjugated antibody to CD123 (Miltenyi Biotec). PBMCs or pDC-depleted PBMCs ($1 \times 10^6$ to $2 \times 10^6$ cells) were stimulated with each influenza vaccine at the indicated concentration. Twenty-four hours later, IFN-α and IFN-γ (R&D Systems) were measured in supernatants by ELISA according to their manufacturers' protocol.

### Statistical analysis

Statistical significance ($P < 0.05$) between groups was determined using the Student's *t* test. A survival curve was generated using Kaplan-Meier methodology, and the susceptibility of mice after infection was compared using the log-rank test.

## SUPPLEMENTARY MATERIAL

www.sciencetranslationalmedicine.org/cgi/content/full/2/25/25ra24/DC1

Materials and Methods

Fig. S1. TLR7-dependent, but not IPS-1–dependent, signaling is required for the induction of protective immune responses with inactivated WV vaccine by i.m. immunization.

Fig. S2. ASC-dependent inflammasome activation was dispensable for adaptive immune response to influenza virus infection, except for systemic IgG1 production.

Fig. S3. Type I IFN receptor–mediated signaling was indispensable for adaptive immune response to WV but not to the live virus.

Fig. S4. Plasmacytoid DC depletion by mPDCA-1 antibody was confirmed in spleen.

Fig. S5. Type I IFN interaction between pDCs and other immune cells was required for WV vaccine immunogenicity.

Fig. S6. Different manner of type I IFN response to WV vaccine and split vaccine is dependent on the presence of the viral genome RNA.

Fig. S7. Indispensable role of type I IFN–mediated signaling in vaccination with split vaccine plus SPG-CpG.

References

## REFERENCES AND NOTES


1. K. L. Nichol, J. J. Treanor, Vaccines for seasonal and pandemic influenza. *J. Infect. Dis.* **194**, S111–S118 (2006).
2. A. E. Fiore, D. K. Shay, K. Broder, J. K. Iskander, T. M. Uyeki, G. Mootrey, J. S. Bresee, N. S. Cox; Centers for Disease Control and Prevention (CDC); Advisory Committee on Immunization Practices (ACIP), Prevention and control of influenza: Recommendations of the Advisory Committee on Immunization Practices (ACIP), 2008. *MMWR Recomm. Rep.* **57**, 1–60 (2008).
3. P. A. Gross, F. A. Ennis, P. F. Gaerlan, L. J. Denson, C. R. Denning, D. Schiffman, A controlled double-blind comparison of reactogenicity, immunogenicity, and protective efficacy of whole-virus and split-product influenza vaccines in children. *J. Infect. Dis.* **136**, 623–632 (1977).
4. P. A. Gross, F. A. Ennis, Influenza vaccine: Split-product versus whole-virus types—How do they differ. *N. Engl. J. Med.* **296**, 567–568 (1977).
5. J. Rhorer, C. S. Ambrose, S. Dickinson, H. Hamilton, N. A. Oleka, F. J. Malinoski, J. Wittes, Efficacy of live attenuated influenza vaccine in children: A meta-analysis of nine randomized clinical trials. *Vaccine* **27**, 1101–1110 (2009).
6. L. Simonsen, R. J. Taylor, C. Viboud, M. A. Miller, L. A. Jackson, Mortality benefits of influenza vaccination in elderly people: An ongoing controversy. *Lancet Infect. Dis.* **7**, 658–666 (2007).
7. F. L. Ruben, Inactivated influenza virus vaccines in children. *Clin. Infect. Dis.* **38**, 678–688 (2004).
8. E. Hak, E. Buskens, G. A. van Essen, D. H. de Bakker, D. E. Grobbee, M. A. Tacken, B. A. van Hout, T. J. Verheij, Clinical effectiveness of influenza vaccination in persons younger than 65 years with high-risk medical conditions: The PRISMA study. *Arch. Intern. Med.* **165**, 274–280 (2005).
9. F. Carrat, A. Flahault, Influenza vaccine: The challenge of antigenic drift. *Vaccine* **25**, 6852–6862 (2007).
10. B. Pulendran, R. Ahmed, Translating innate immunity into immunological memory: Implications for vaccine development. *Cell* **124**, 849–863 (2006).
11. N. W. Palm, R. Medzhitov, Pattern recognition receptors and control of adaptive immunity. *Immunol. Rev.* **227**, 221–233 (2009).
12. K. J. Ishii, S. Akira, Toll or toll-free adjuvant path toward the optimal vaccine development. *J. Clin. Immunol.* **27**, 363–371 (2007).
13. S. Koyama, K. J. Ishii, H. Kumar, T. Tanimoto, C. Coban, S. Uematsu, T. Kawai, S. Akira, Differential role of TLR- and RLR-signaling in the immune responses to influenza A virus infection and vaccination. *J. Immunol.* **179**, 4711–4720 (2007).
14. T. Ichinohe, H. K. Lee, Y. Ogura, R. Flavell, A. Iwasaki, Inflammasome recognition of influenza virus is essential for adaptive immune responses. *J. Exp. Med.* **206**, 79–87 (2009).
15. S. Koyama, C. Coban, T. Aoshi, T. Horii, S. Akira, K. J. Ishii, Innate immune control of nucleic acid-based vaccine immunogenicity. *Expert Rev. Vaccines* **8**, 1099–1107 (2009).
16. S. S. Diebold, T. Kaisho, H. Hemmi, S. Akira, C. Reis e Sousa, Innate antiviral responses by means of TLR7-mediated recognition of single-stranded RNA. *Science* **303**, 1529–1531 (2004).
17. A. Pichlmair, O. Schulz, C. P. Tan, T. I. Näslund, P. Liljeström, F. Weber, C. Reis e Sousa, RIG-I-mediated antiviral responses to single-stranded RNA bearing 5′-phosphates. *Science* **314**, 997–1001 (2006).
18. I. C. Allen, M. A. Scull, C. B. Moore, E. K. Holl, E. McElvania-TeKippe, D. J. Taxman, E. H. Guthrie, R. J. Pickles, J. P. Ting, The NLRP3 inflammasome mediates in vivo innate immunity to influenza A virus through recognition of viral RNA. *Immunity* **30**, 556–565 (2009).
19. P. G. Thomas, P. Dash, J. R. Aldridge Jr., A. H. Ellebedy, C. Reynolds, A. J. Funk, W. J. Martin, M. Lamkanfi, R. J. Webby, K. L. Boyd, P. C. Doherty, T. D. Kanneganti, The intracellular sensor NLRP3 mediates key innate and healing responses to influenza A virus via the regulation of caspase-1. *Immunity* **30**, 566–575 (2009).
20. S. M. Santini, C. Lapenta, M. Logozzi, S. Parlato, M. Spada, T. Di Pucchio, F. Belardelli, Type I interferon as a powerful adjuvant for monocyte-derived dendritic cell development and activity in vitro and in Hu-PBL-SCID mice. *J. Exp. Med.* **191**, 1777–1788 (2000).
21. A. Le Bon, G. Schiavoni, G. D'Agostino, I. Gresser, F. Belardelli, D. F. Tough, Type I interferons potently enhance humoral immunity and can promote isotype switching by stimulating dendritic cells in vivo. *Immunity* **14**, 461–470 (2001).

22. T. Mizukami, J. Imai, I. Hamaguchi, M. Kawamura, H. Momose, S. Naito, J. Maeyama, A. Masumi, M. Kuramitsu, K. Takizawa, N. Nomura, S. Watanabe, K. Yamaguchi, Application of DNA microarray technology to influenza A/Vietnam/1194/2004 (H5N1) vaccine safety evaluation. *Vaccine* **26**, 2270–2283 (2008).
23. G. E. Price, A. Gaszewska-Mastarlarz, D. Moskophidis, The role of α/β and γ interferons in development of immunity to influenza A virus in mice. *J. Virol.* **74**, 3996–4003 (2000).
24. M. Colonna, G. Trinchieri, Y. J. Liu, Plasmacytoid dendritic cells in immunity. *Nat. Immunol.* **5**, 1219–1226 (2004).
25. A. Krug, A. R. French, W. Barchet, J. A. Fischer, A. Dzionek, J. T. Pingel, M. M. Orihuela, S. Akira, W. M. Yokoyama, M. Colonna, TLR9-dependent recognition of MCMV by IPC and DC generates coordinated cytokine responses that activate antiviral NK cell function. *Immunity* **21**, 107–119 (2004).
26. C. H. GeurtsvanKessel, M. A. Willart, L. S. van Rijt, F. Muskens, M. Kool, C. Baas, K. Thielemans, C. Bennett, B. E. Clausen, H. C. Hoogsteden, A. D. Osterhaus, G. F. Rimmelzwaan, B. N. Lambrecht, Clearance of influenza virus from the lung depends on migratory langerin$^{+}$CD11b$^{-}$ but not plasmacytoid dendritic cells. *J. Exp. Med.* **205**, 1621–1634 (2008).
27. A. I. Wolf, D. Buehler, S. E. Hensley, L. L. Cavanagh, E. J. Wherry, P. Kastner, S. Chan, W. Weninger, Plasmacytoid dendritic cells are dispensable during primary influenza virus infection. *J. Immunol.* **182**, 871–879 (2009).
28. F. Geeraedts, N. Goutagny, V. Hornung, M. Severa, A. de Haan, J. Pool, J. Wilschut, K. A. Fitzgerald, A. Huckriede, Superior immunogenicity of inactivated whole virus H5N1 influenza vaccine is primarily controlled by Toll-like receptor signalling. *PLoS Pathog.* **4**, e1000138 (2008).
29. N. Shimada, K. J. Ishii, Y. Takeda, C. Coban, Y. Torii, S. Shinkai, S. Akira, K. Sakurai, Synthesis and in vitro characterization of antigen-conjugated polysaccharide as a CpG DNA carrier. *Bioconjug. Chem.* **17**, 1136–1140 (2006).
30. L. Franchi, T. Eigenbrod, R. Muñoz-Planillo, G. Nuñez, The inflammasome: A caspase-1-activation platform that regulates immune responses and disease pathogenesis. *Nat. Immunol.* **10**, 241–247 (2009).
31. J. A. Greenbaum, M. F. Kotturi, Y. Kim, C. Oseroff, K. Vaughan, N. Salimi, R. Vita, J. Ponomarenko, R. H. Scheuermann, A. Sette, B. Peters, Pre-existing immunity against swine-origin H1N1 influenza viruses in the general human population. *Proc. Natl. Acad. Sci. U.S.A.* **106**, 20365–20370 (2009).
32. X. Ge, V. Tan, P. L. Bollyky, N. E. Standifer, E. A. James, W. W. Kwok, Assessment of seasonal influenza A virus-specific CD4 T-cell responses to 2009 pandemic H1N1 swine-origin influenza A virus. *J. Virol.* **84**, 3312–3319 (2010).
33. L. Y. Lee, L. A. Ha do, C. Simmons, M. D. de Jong, N. V. Chau, R. Schumacher, Y. C. Peng, A. J. McMichael, J. J. Farrar, G. L. Smith, A. R. Townsend, B. A. Askonas, S. Rowland-Jones, T. Dong, Memory T cells established by seasonal human influenza A infection cross-react with avian influenza A (H5N1) in healthy individuals. *J. Clin. Invest.* **118**, 3478–3490 (2008).
34. M. Smallman-Raynor, A. D. Cliff, Avian influenza A (H5N1) age distribution in humans. *Emerg. Infect. Dis.* **13**, 510–512 (2007).
35. T. Reichert, G. Chowell, H. Nishiura, R. A. Christensen, J. A. McCullers, Does glycosylation as a modifier of Original Antigenic Sin explain the case age distribution and unusual toxicity in pandemic novel H1N1 influenza? *BMC Infect. Dis.* **10**, 5 (2010).
36. X. S. He, T. H. Holmes, C. Zhang, K. Mahmood, G. W. Kemble, D. B. Lewis, C. L. Dekker, H. B. Greenberg, A. M. Arvin, Cellular immune responses in children and adults receiving inactivated or live attenuated influenza vaccines. *J. Virol.* **80**, 11756–11766 (2006).
37. H. J. Ehrlich, M. Müller, H. M. Oh, P. A. Tambyah, C. Joukhadar, E. Montomoli, D. Fisher, G. Berezuk, S. Fritsch, A. Löw-Baselli, N. Vartian, R. Bobrovsky, B. G. Pavlova, E. M. Pöllabauer, O. Kistner, P. N. Barrett; Baxter H5N1 Pandemic Influenza Vaccine Clinical Study Team, A clinical trial of a whole-virus H5N1 vaccine derived from cell culture. *N. Engl. J. Med.* **358**, 2573–2584 (2008).
38. J. Lin, J. Zhang, X. Dong, H. Fang, J. Chen, N. Su, Q. Gao, Z. Zhang, Y. Liu, Z. Wang, M. Yang, R. Sun, C. Li, S. Lin, M. Ji, Y. Liu, X. Wang, J. Wood, Z. Feng, Y. Wang, W. Yin, Safety and immunogenicity of an inactivated adjuvanted whole-virion influenza A (H5N1) vaccine: A phase I randomised controlled trial. *Lancet* **368**, 991–997 (2006).
39. T. J. Powell, T. Strutt, J. Reome, J. A. Hollenbaugh, A. D. Roberts, D. L. Woodland, S. L. Swain, R. W. Dutton, Priming with cold-adapted influenza A does not prevent infection but elicits long-lived protection against supralethal challenge with heterosubtypic virus. *J. Immunol.* **178**, 1030–1038 (2007).
40. S. R. Mostow, T. C. Eickhoff, G. A. Chelgren, H. F. Retailliau, M. Castle, Studies of inactivated influenza virus vaccines in hospital employees: Reactogenicity and absenteeism. *J. Infect. Dis.* **136**, S533–S538 (1977).
41. E. Greenbaum, D. Engelhard, R. Levy, M. Schlezinger, A. Morag, Z. Zakay-Rones, Mucosal (SIgA) and serum (IgG) immunologic responses in young adults following intranasal administration of one or two doses of inactivated, trivalent anti-influenza vaccine. *Vaccine* **22**, 2566–2577 (2004).
42. S. Tamura, T. Kurata, Defense mechanisms against influenza virus infection in the respiratory tract mucosa. *Jpn. J. Infect. Dis.* **57**, 236–247 (2004).
43. M. Muszkat, E. Greenbaum, A. Ben-Yehuda, M. Oster, E. Yeu'l, S. Heimann, R. Levy, G. Friedman, Z. Zakay-Rones, Local and systemic immune response in nursing-home elderly following intranasal or intramuscular immunization with inactivated influenza vaccine. *Vaccine* **21**, 1180–1186 (2003).
44. R. L. Atmar, W. A. Keitel, T. R. Cate, F. M. Munoz, F. Ruben, R. B. Couch, A dose–response evaluation of inactivated influenza vaccine given intranasally and intramuscularly to healthy young adults. *Vaccine* **25**, 5367–5373 (2007).
45. A. Takada, S. Matsushita, A. Ninomiya, Y. Kawaoka, H. Kida, Intranasal immunization with formalin-inactivated virus vaccine induces a broad spectrum of heterosubtypic immunity against influenza A virus infection in mice. *Vaccine* **21**, 3212–3218 (2003).
46. K. J. Ishii, T. Kawagoe, S. Koyama, K. Matsui, H. Kumar, T. Kawai, S. Uematsu, O. Takeuchi, F. Takeshita, C. Coban, S. Akira, TANK-binding kinase-1 delineates innate and adaptive immune responses to DNA vaccines. *Nature* **451**, 725–729 (2008).
47. S. Mariathasan, D. S. Weiss, K. Newton, J. McBride, K. O'Rourke, M. Roose-Girma, W. P. Lee, Y. Weinrauch, D. M. Monack, V. M. Dixit, Cryopyrin activates the inflammasome in response to toxins and ATP. *Nature* **440**, 228–232 (2006).
48. T. Tanimoto, R. Nakatsu, I. Fuke, T. Ishikawa, M. Ishibashi, K. Yamanishi, M. Takahashi, S. Tamura, Estimation of the neuraminidase content of influenza viruses and split-product vaccines by immunochromatography. *Vaccine* **23**, 4598–4609 (2005).
49. N. Shimada, C. Coban, Y. Takeda, M. Mizu, J. Minari, T. Anada, Y. Torii, S. Shinkai, S. Akira, K. J. Ishii, K. Sakurai, A polysaccharide carrier to effectively deliver native phosphodiester CpG DNA to antigen-presenting cells. *Bioconjug. Chem.* **18**, 1280–1286 (2007).
50. M. Mizu, K. Koumoto, T. Anada, T. Matsumoto, M. Numata, S. Shinkai, T. Nagasaki, K. Sakurai, A polysaccharide carrier for immunostimulatory CpG DNAs to enhance cytokine secretion. *J. Am. Chem. Soc.* **126**, 8372–8373 (2004).



51. **Acknowledgments:** We thank T. Nukiwa, S. Uematsu, F. Takeshita, H. Kumar, T. Kawai, Y. Kawaoka, and T. Nakaya for providing critical materials and helpful suggestions. **Funding:** Japan Society for the Promotion of Science Research Fellowships for Young Scientists (S.K.); Knowledge Cluster Initiative (K.J.I. and T.H.); Grant-in-Aid for Scientific Research (KAKENHI) (K.J.I. and C.C.); Target protein project (K.J.I. and S.A.); Ministry of Education, Culture, Sports, Science and Technology; and Core Research for Evolutional Science and Technology, Japan Science and Technology Agency (K.S. and K.J.I.). **Competing interests:** Some of the authors have filed a patent application: Immunostimulatory DNA complex with β-1,3-D-glucan. Inventors: K.S., S. Shinkai, N. Shimada, K.J.I., and S.A. Applicant ERATO, SORST/JST JP2006-282148. The authors declare no other competing interests.

Submitted 22 December 2009
Accepted 11 March 2010
Published 31 March 2010
10.1126/scitranslmed.3000759

**Citation:** S. Koyama, T. Aoshi, T. Tanimoto, Y. Kumagai, K. Kobiyama, T. Tougan, K. Sakurai, C. Coban, T. Horii, S. Akira, K. J. Ishii, Plasmacytoid dendritic cells delineate immunogenicity of influenza vaccine subtypes. *Sci. Transl. Med.* **2**, 25ra24 (2010).

# NLRP4 Negatively Regulates Autophagic Processes through an Association with Beclin1

Nao Jounai,*,[1] Kouji Kobiyama,*,[1] Masaaki Shiina,[†] Kazuhiro Ogata,[†] Ken J. Ishii,[‡,§] and Fumihiko Takeshita*

**Although more than 20 putative members have been assigned to the nucleotide-binding and oligomerization domain-like receptor (NLR) family, their physiological and biological roles, with the exception of the inflammasome, are not fully understood. In this article, we show that NLR members, such as NLRC4, NLRP3, NLRP4, and NLRP10 interact with Beclin1, an important regulator of autophagy, through their neuronal apoptosis inhibitory protein, MHC class II transcription activator, incompatibility locus protein from *Podospora anserina*, and telomerase-associated protein domain. Among such NLRs, NLRP4 had a strong affinity to the Beclin1 evolutionally conserved domain. Compromising NLRP4 via RNA interference resulted in upregulation of the autophagic process under physiological conditions and upon invasive bacterial infections, leading to enhancement of the autophagic bactericidal process of group A streptococcus. NLRP4 recruited to the subplasma membrane phagosomes containing group A streptococcus and transiently dissociated from Beclin1, suggesting that NLRP4 senses bacterial infection and permits the initiation of Beclin1-mediated autophagic responses. In addition to a role as a negative regulator of the autophagic process, NLRP4 physically associates with the class C vacuolar protein-sorting complex, thereby negatively regulating maturation of the autophagosome and endosome. Collectively, these results provide novel evidence that NLRP4, and possibly other members of the NLR family, plays a crucial role in biogenesis of the autophagosome and its maturation by the association with regulatory molecules, such as Beclin1 and the class C vacuolar protein-sorting complex.** *The Journal of Immunology*, **2011, 186: 1646–1655.**

Atg5/Atg7-dependent macroautophagy (referred to as autophagy in this article), an intracellular protein-degradation system required for cellular homeostasis, regulates the sequestration and elimination of some types of intracellular bacteria (1–3). Following entry into host phagocytic cells, invasive pathogens, such as group A streptococcus (GAS; *Streptococcus pyogenes*) and *Listeria monocytogenes*, escape from the conventional phagosome by digesting its membrane with the secreted hemolytic enzymes streptolysin O and listeriolysin O, respectively (4, 5). Once bacteria are released into the cytoplasm, they are captured by the autophagosomes, whose double-membrane structure is resistant to lytic bacterial enzymes. Subsequently, the autophagosomes mature by fusion with the lysosomes, and bacteria present within autolysosomes are killed and digested. Cells that are deficient for this autophagic process are incapable of eliminating such invasive bacteria; thus, the autophagic bactericidal process is crucial for cell-autonomous antibacterial resistance.

Mechanisms underlying the initiation of autophagy have been extensively investigated over the past decade. Recent evidence indicates that one of the key initiators of the autophagic process is Beclin1, which associates with PI3K class III (PI3KC3), thereby mediating biogenesis and dynamics of subcellular membranes involved in autophagy. Additionally, it was demonstrated that binding partners of Beclin1, such as the activating molecule in Beclin1-regulated autophagy (Ambra1), UV radiation resistance-associated gene protein (UVRAG), and Atg14L, positively regulate autophagy, whereas Bcl-2, originally identified as an inhibitory factor for apoptosis signaling, inhibits autophagy (6–9). UVRAG was shown to play another biological role by interacting with the class C vacuolar protein sorting (C-VPS) complex, consisting of VPS11, VPS16 and VPS18, and facilitating the activation of Rab7 on the Rab5-labeled vacuole. This is known as Rab conversion during maturation of the autophagosome, as well as the endosome (10). Furthermore, a recent study demonstrated that Run domain protein as Beclin1 interacting and cysteine-rich containing (Rubicon) inhibits the maturation process of the autophagosome (8, 9). Taken together, it was suggested that the several

*Department of Molecular Biodefense Research, Yokohama City University Graduate School of Medicine, Yokohama 236-0004, Japan; [†]Department of Biochemistry, Yokohama City University Graduate School of Medicine, Yokohama 236-0004, Japan; [‡]Laboratory of Host Defense, World Premier International Immunology Frontier Research Center, Osaka University, Suita 565-8701, Japan; and [§]Department of Molecular Protozoology, Research Institute for Microbial Diseases, Osaka University, Suita 565-8701, Japan

[1]N.J. and K.K. contributed equally to this work.

Received for publication May 27, 2010. Accepted for publication November 30, 2010.

This work was supported in part by a grant-in-aid for scientific research from the Ministry of Education, Culture, Sports, Science, and Technology of Japan (#20590477 and #20200074 to F.T.). This work was also supported by a grant-in-aid from Yokohama Foundation for Advancement of Medical Science (to N.J.).

N.J., K.K., K.J.I., and F.T. designed the experiments; N.J., K.K., M.S., and F.T. performed the outlined research experiments; K.J.I., K.O., and F.T. analyzed data; and N.J., K.K., K.J.I., and F.T. wrote the manuscript.

Address correspondence and reprint requests to Dr. Fumihiko Takeshita, Department of Molecular Biodefense Research, Yokohama City University Graduate School of Medicine, 3-9 Fukuura Kanazawaku, Yokohama 236-0004, Japan. E-mail address: takesita@yokohama-cu.ac.jp

The online version of this article contains supplemental material.

Abbreviations used in this article: BD, Bcl-2 binding domain; CCD, coiled-coil domain; C-VPS, class C vacuolar protein sorting; ECD, evolutionally conserved domain; EGF, epidermal growth factor; EGFR, epidermal growth factor receptor; GAS, group A streptococcus; GcAV, group A streptococcus-containing autophagosome-like vacuole; MOI, multiplicity of infection; NACHT, neuronal apoptosis inhibitory protein, MHC class II transcription activator, incompatibility locus protein from *Podospora anserina*, and telomerase-associated protein; NLR, nucleotide-binding and oligomerization domain-like receptor; PI3KC3, PI3K class III; siRNA, small interfering RNA; THY medium, Todd Hewitt medium supplemented with yeast extract; UVRAG, UV radiation resistance-associated gene protein; VSV, vesicular stomatitis virus; WT, wild-type.



www.jimmunol.org/cgi/doi/10.4049/jimmunol.1001654

binding partners of Beclin1 have at least two functions during the autophagic process, thereby controlling autophagic flux. The first function seems to be control of Beclin1-mediated initiation of autophagy, and the second is control of the maturation process of the autophagosome.

Nucleotide-binding and oligomerization domain-like receptors (NLRs) are categorized as a family of cytosolic proteins having structurally conserved domains. This protein family consists of 23 putative members that have been identified in humans and 34 that have been identified in mice. According to a genome-wide analysis of the putative genes, all have several shared domains, such as neuronal apoptosis inhibitory protein, MHC class II transcription activator, incompatibility locus protein from *Podospora anserina*, and telomerase-associated protein (NACHT) domain, pyrin domain, the caspase recruitment domain, and the leucine-rich repeat domain. Some NLR family members, such as NLRC4, NLRP1, and NLRP3, were shown to form an ~700-kDa cytoplasmic protein complex, called an inflammasome, to facilitate the maturation and secretion of proinflammatory cytokines, including IL-1β, IL-18, and IL-33, in response to bacterial infections (11). It was shown that autophagy and a distinct type of cell death process, termed "pyroptosis," are upregulated in NLRC4$^{-/-}$ macrophages relative to wild-type (WT) macrophages postinfection with *Shigella*, suggesting that NLRC4 negatively regulates autophagy and the induction of cell-autonomous bactericidal processes (12).

In the current study, we examined the molecular mechanisms underlying the association between NLR family members and the Beclin1-mediated autophagic bactericidal process. Our results demonstrated that NLRC4 and NLRP4 negatively regulate autophagic processes through an association with Beclin1. In addition, NLRP4 physically interacts with the C-VPS complex, thereby blocking maturation of autophagosomes to autolysosomes. Furthermore, NLRP4 is recruited to and accumulates in the bacteria-containing phagosomes and transiently dissociates from Beclin1 after GAS infection. Our results suggested that NLRP4 is engaged in the mechanism controlling the autophagic flux crucial for the cell-autonomous antibacterial resistance.

## Materials and Methods

### *Cells, bacteria, and reagents*

HEK293, THP-1, and HeLa cells were purchased from the American Type Culture Collection. HEK293 and HeLa cells were maintained in DMEM, whereas THP-1 cells were maintained in RPMI 1640 supplemented with FCS and 50 mg/ml each penicillin and streptomycin. The normal primary HUVECs were purchased from TAKARA (Japan). HUVECs were maintained in the supplemented endothelial cell growth medium-2 without antibiotics, according to the manufacturer's instruction. GAS serotype M6 was a kind gift from E. Hanski (The Hebrew University, Hadassah Medical School, Jerusalem, Israel). GAS was cultured in Todd Hewitt medium supplemented with yeast extract (THY medium) (BD Biosciences). For infection experiments, GAS was prepared by adjusting to 1 $OD_{590}$ (~$1 \times 10^9$ cells/ml) and washing twice with PBS before infection. *L. monocytogenes* were grown in brain/heart infusion broth (BD Biosciences) at 37°C. For infection experiments, *L. monocytogenes* were prepared by adjusting to 1 $OD_{600}$ (~$2 \times 10^9$ cells/ml) and washing twice with PBS before infection. Vesicular stomatitis virus (VSV) was provided by the National Institute of Animal Health (Tokyo, Japan). Cell transfection and RNA interference were performed as described previously (13). The dsRNA for knockdown of *NLRC4* and *NLRP4* was obtained from Invitrogen (stealth RNAi). Each knockdown of *NLRC4* or *NLRP4* was performed with pooled dsRNAs whose sequences are shown in Supplemental Table I. Control small interfering RNA (siRNA) was purchased from Invitrogen (cat. #12935-300). Primers (Supplemental Table II) were used to confirm the level of RNA encoding *NLRC4* and *NLRP4*. In some cases, cotransfection with expression plasmid and siRNA was performed by Lipofectamine 2000 (Invitrogen), according to the manufacturer's instructions.

### *Gel-filtration assay*

HeLa cells were disrupted as described previously (14), and the cytoplasmic lysate was subjected to size fractionation with Superdex 200 (GE Healthcare).

### *Plasmids*

NLRC4, NLRP3, NLRP4, NLRP10, Beclin1, p57, VPS11, VPS16, VPS18, and LC3 cDNAs were amplified by PCR using a human or mouse spleen cDNA library. The cDNA fragments were introduced into pFLAG-CMV4, pFLAG-CMV5 (Sigma), pCIneo (Promega), pCIneo-HA, or pCAGGS-CFP (15). Each truncated protein was prepared by insertion of the following PCR amplicons into expression vector plasmids: NLRC4 caspase recruitment domain (1–100), NLRC4 NACHT (100–500), NLRP3 NACHT (200–550), NLRP4 NACHT (100–500), NLRP10 NACHT (140–500), Beclin1 BD (90–152), Beclin1 CCD (152–246), and Beclin1 ECD (246–339). To construct the mRFP-GFP-LC3–expressing plasmid, open reading frames of mRFP, GFP, and LC3 were tandemly ligated and introduced into pCIneo. For generation of recombinant lentiviruses, the targeting cDNA was introduced into CSII-CMV-MCS-IRES-puro or CSII-EF-MCS-IRES-hyg (16, 17) to obtain CS-mRFP-GFP-LC3-IRES-puro, CS-CFP-NLRP4-IRES-hyg, and CS-CFP-p57-IRES-hyg.

### *Immunoprecipitation and immunoblotting*

Immunoprecipitation assays were performed as described previously (18). Immunoblotting analyses were performed using anti-LC3 (Cell Signaling, cat. #2775), anti-Beclin1 (AnaSpec), anti–β-actin (Cell Signaling Technology), anti-NLRC4 (AnaSpec, cat. #54128), anti-NLRP4 (IMGENEX, cat. #IMG-5743), anti-p62 (BIOMOL, cat. #PW9860), anti-FLAG M2 (Sigma), or anti-HA (Roche Diagnostics), as described previously (18). For reprobing the membrane with different Abs, the membrane was incubated in stripping buffer (400 mM glycine, 0.2% SDS, 2% Tween 20 [pH 2.2]) for 10 min at room temperature, washed, and Ab was added to the membrane. To detect human NLRC4 and NLRP4 protein, Can Get Signal (TOYOBO) was used to augment the signal.

### *RT-PCR*

Total RNA was extracted with TRIzol reagent (Invitrogen), according to the manufacturer's instructions. Extracted total RNA was reverse transcribed with ReverTra Ace reverse transcriptase (TOYOBO), and standard PCR was conducted as described previously (19).

### *Quantitative RT-PCR*

SYBR Green technology was applied for all of the assays with ABI 7500 standard quantitative PCR system (Applied Biosystems, CA). SYBR Premix Ex Taq II was purchased from TAKARA (Japan). Primer pairs are listed in Supplemental Table III. The *gapdh* gene was used as an internal control.

### *Cytokine ELISA*

Human IL-1β was quantified with the Human IL-1β/IL-1F2 DuoSet (R&D Systems), according to the manufacturer's instruction.

### *Evaluation of bacterial viability*

The bacteria grown until midlog phase were harvested and washed twice with PBS (pH 7.4) and then adjusted to appropriate cell density. The bacteria were added to cell cultures ($1 \times 10^5$ HeLa cells or $2 \times 10^5$ HUVECs in a 12-well culture plate) at a multiplicity of infection (MOI) of 50 without antibiotics. One hour postinfection, antibiotics (penicillin and streptomycin) were added to the culture medium to kill extracellular bacteria, and the cells were further cultured for the indicated time periods. After an appropriate incubation time, infected cells were lysed in 1 ml sterile distilled water, and serial dilutions of the lysates were plated on THY agar plates. The colony numbers were enumerated 24 h after plating. Data represent the mean ± SD of recovered bacteria for three independent experiments.

### *Generation of stably transformed HeLa cells*

Recombinant lentiviruses expressing mRFP-GFP-LC3, CFP-NLRP4, or CFP-p57 were generated by transfecting CS-mRFP-GFP-LC3-IRES-puro, CS-CFP-NLRP4-IRES-hyg, or CS-CFP-p57-IRES-hyg, as well as pCAG-HIVgp and pCMV-VSV-G-RSV-Rev, into HEK293 cells, as described in another study (20). Forty-eight to seventy-two hours following transfection, the culture supernatants were recovered and transferred to the fresh HeLa cell culture. HeLa cells expressing mRFP-GFP-LC3, CFP-

NLRP4, or CFP-p57 were selected in the presence of puromycin (2 mg/ml) alone or puromycin plus hygromycin (200 mg/ml).

*Fluorescent and confocal microscopy analysis*

Fluorescent microscopy analysis was performed with a fluorescent deconvolution microscope (BIOZERO; Keyence, Japan). Confocal microscopy analysis was performed with FLUOVIEW FV1000-D (BX61WI; OLYMPUS). For immunofluorescent staining of GAS, HeLa cells were fixed and immunostained with an anti-GAS Ab (Abcam), followed by an Alexa Fluor 546-conjugated anti-rabbit IgG (Invitrogen) secondary Ab, and were subjected to microscopy analysis.

*Epidermal growth factor receptor degradation assay*

Control, NLRC4-knockdown, or NLRP4-knockdown HeLa cells were treated with 200 ng/ml recombinant epidermal growth factor (EGF) (R&D Systems) for the indicated periods and were subjected to immunoblotting analysis with the anti-EGF receptor (EGFR) (1005; Santa Cruz).

*Statistical analysis*

The Student *t* test was used for statistical analysis.

## Results

*NLR family members interact with Beclin1*

To assess possible roles for NLR family members in the autophagic process, their molecular interactions with Beclin1, the primary regulator of autophagy, was examined by immunoprecipitation analysis. As a result, NLRC4, NLRP3, NLRP4, NLRP10, and NOD2, but not GFP, coprecipitated with Beclin1 in HEK293 and HeLa cells, suggesting that these NLR family members have the potential to interact with Beclin1 (Fig. 1*A*, Supplemental Fig. 1*A*, 1*B*). Additionally, a NACHT domain of each NLR was shown to be sufficient for interaction with Beclin1 (Fig. 1*B*). The highest levels of such an interaction were seen between NLRP4 NACHT and Beclin1 (Fig. 1*B*). The NACHT domain of NLRC4 was shown to catalyze nucleotide hydrolysis through direct interaction with ATP/2′deoxyadenosine triphosphate, crucial for self-multimerization, caspase-1 activation, and subsequent IL-1β release as a function of the inflammasome. In contrast to such previous observations, the loss-of-function mutant NLRC4 NACHT K175R was shown to interact with Beclin1 comparably to WT NLRC4, suggesting that ATP/2′deoxyadenosine triphosphate binding is not essential for NACHT domain interaction with Beclin1 (Fig. 1*B*). We further examined the endogenous interaction between NLRP4 and Beclin1 in HeLa cells or the normal primary HUVECs. As a result, NLRP4 was shown to interact with Beclin1 under physiological conditions (Fig. 1*C*, Supplemental Fig. 2).

Although endogenous human NLRP4 protein could be recognized at the expected size upon immunoblotting, little is known about the expression of human NLRP4. To strengthen NLRP4 expression in HeLa cells and HUVECs, we evaluated *NLRP4*-encoding RNA level (Supplemental Fig. 3*A*, 3*B*). The *NLRP4*-encoding RNA could be detected in HeLa cells and HUVECs by RT-PCR (Supplemental Fig. 3*A*). To quantify *NLRP4*-encoding RNA level by quantitative PCR, we evaluated it compared with the expression level of NLRC4, because its expression at the RNA and protein levels has been reported (21). As shown in Supplemental Fig. 3*B*, the level of *NLRP4*-encoding RNA was 6-fold lower than that of *NLRC4* in HeLa cells. However, the RNA level of *NLRP4* in HUVECs was comparable to that of *NLRC4* in HeLa cells and slightly less than that of *NLRC4* in HUVECs (Supplemental Fig. 3*B*). It suggests that *NLRP4*'s expression level might vary among cell types, and *NLRP4* in HUVECs was expressed at the same RNA level as *NLRC4* in HeLa cells (Supplemental Fig. 3*B*).

Beclin1 was shown to interact with several autophagy regulators via distinct interaction domains: the Bcl-2 binding domain (BD), the coiled-coil domain (CCD), and the evolutionally conserved domain (ECD), whose structure is uncharacterized but highly conserved among Beclin1 zoologues. When each Beclin1 domain (BD, CCD, ECD) was ectopically expressed in HEK293 cells, the levels of ECD protein were relatively low (Fig. 1*D*). Nonetheless, the level of each NACHT domain that coprecipitated with Beclin1 ECD was higher than those with Beclin1 BD or CCD, suggesting that Beclin1 ECD has a high affinity for the NLR NACHT domains (Fig. 1*D*). Consistent with the result shown in Fig. 1*B*, the NLRP4 NACHT domain most strongly interacted with the Beclin1 ECD (Fig. 1*D*). Furthermore, we characterized several point mutants of the NLRP4 NACHT domain and found that NLRP4 NACHT W345A or W405A was incapable of interacting with Beclin1, suggesting that the structure conformed by these Trp residues confers the interaction between the NLRP4 NACHT domain and Beclin1 ECD (Fig. 1*E*).

It was shown that Beclin1 physiologically interacts with a variety of cytoplasmic proteins, forming different types of molecular complexes (6). To examine whether NLRP4 also forms the complexes in the cells, HeLa cells were mechanically disrupted, and the cytoplasmic lysate was size fractionated by gel filtration. The presence of Beclin1 (52 kDa) and NLRP4 (113 kDa) in each fraction was examined by immunoblotting. Beclin1 was found in fractions 3–6 comprising molecules of 400–700 kDa, consistent with a previous report (Fig. 1*F*) (8). NLRP4 was found in fractions 4 and 5, suggesting that NLRP4 might be present in the 500–700-kDa cytoplasmic complex containing Beclin1 (Fig. 1*C*, 1*F*).

*The NLR NACHT domain promotes the interaction between Beclin1 and the heterologous NACHT domain*

The NLR NACHT domains were suggested to play a role in self-multimer formation, which is crucial for inflammasome activation. As shown in Fig. 2*A*, FLAG-NLRP4 interacted with HA-NLRC4, HA-NLRP3, HA-NLRP4, or HA-NLRP10. Among these, FLAG-NLRP4 showed the highest levels of interaction with HA-NLRP4, suggesting that NLRP4 preferentially forms the homologous multimer. Similarly, the NACHT domains of these NLR family members were sufficient for association with the NACHT domain of NLRP4 (Fig. 2*B*). The NLRP4 NACHT W345A and W405A, which are not capable of binding to Beclin1, also interacted with the homologous WT NACHT domain (Fig. 2*B*), suggesting that the structural bases are different between NACHT–NACHT and NACHT–Beclin1 interactions. We then examined whether a multimer formation between different NLR family members modulates NLR interaction with Beclin1. Although the interaction between NLRP4 and NLRC4 was weak (Fig. 2*A*), the degree of NLRP4 interaction with Beclin1 ECD increased as a result of NLRC4 concomitantly interacting with Beclin1 ECD in a dose-dependent fashion (Fig. 2*C*). A similar result was observed involving the NACHT domains of NLRC4 and NLRP4 (Fig. 2*D*), suggesting that the NLRP4 NACHT domain facilitates the interaction between Beclin1 and the heterologous NACHT domain. We also examined whether overexpression of Beclin1 ECD leads to upregulation of autophagy by dissociating NLRP4 from Beclin1. However, as a result, neither the number of LC3 vacuoles nor the levels of p62, an intracellular protein specifically and constitutively degraded by autophagic process (22), changed following Beclin1 ECD overexpression (Supplemental Fig. 4*A*, 4*B*).

*Knockdown of NLRC4 or NLRP4 promotes the autophagic process*

Based on experiments investigating the association between NLR family molecules and Beclin1, NLRP4 NACHT domain showed a stronger affinity with Beclin1 ECD than other NLR NACHT

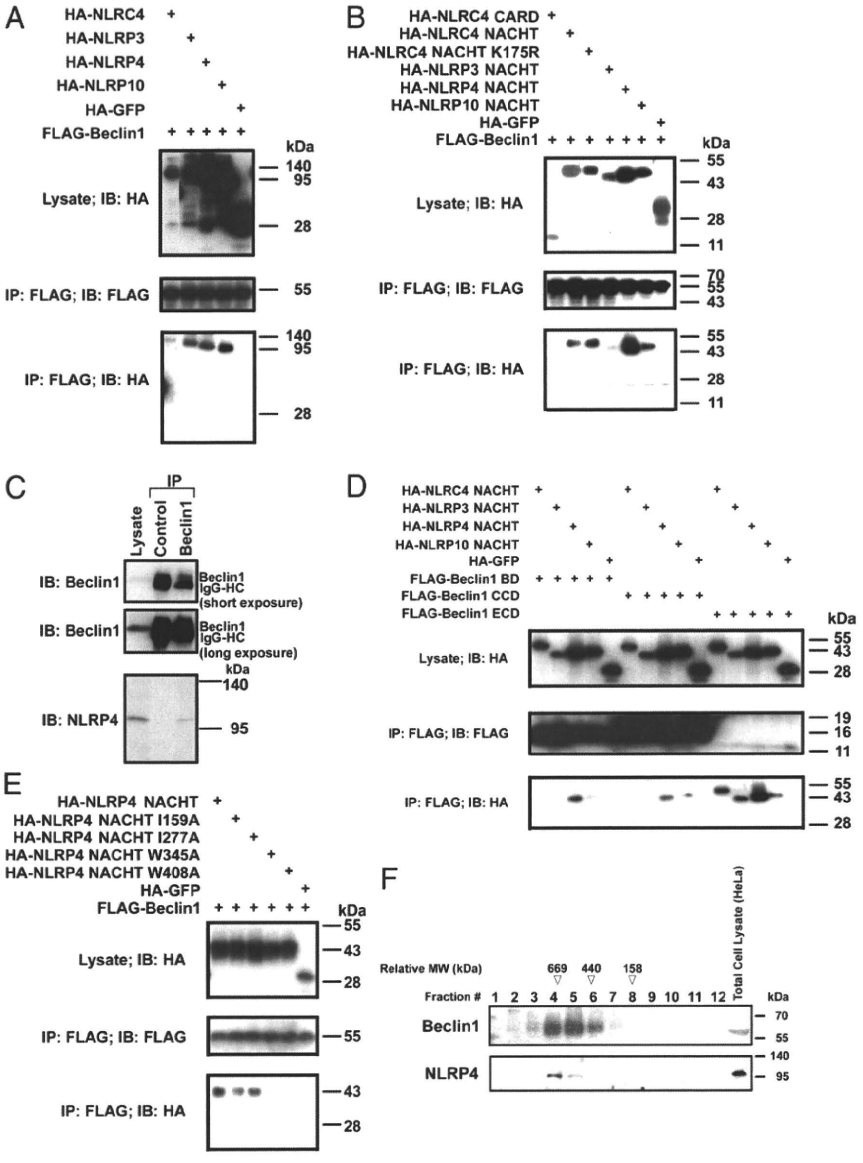


**FIGURE 1.** The NLR family of proteins interacts with Beclin1 through the NLR NACHT domain and Beclin1 ECD. *A*, *B*, *D*, and *E*, HEK293 cells were transfected with the indicated plasmids. Forty-eight hours posttransfection, cells were subjected to immunoprecipitation and immunoblotting analyses. *C*, Six million HeLa cells were lysed, endogenous Beclin1 was immunoprecipitated, and the associated levels of NLRP4 were immunoblotted. *F*, HeLa cells were mechanically disrupted, and the lysate was fractioned with Sephadex 200. The expression level of Beclin1 or NLRP4 in each fraction was examined by immunoblotting. Representative results from at least three independent experiments are shown.

domains (Fig. 1*B*, 1*D*), indicating that NLRP4 might strongly influence the induction and/or magnitude of autophagy. To examine the roles of NLRP4 in the autophagic process, NLRC4 or NLRP4 mRNA was ablated by RNA interference. The levels of RNA encoding endogenous NLRC4 or NLRP4 were specifically decreased by siRNA treatment in HeLa cells (Fig. 3*A*). The knockdown efficiency by NLRP4 siRNA was also confirmed at endogenous protein levels (Fig. 3*B*, Supplemental Fig. 5). To monitor the levels of the autophagic process, the levels of LC3 conversion were examined in the cells pretreated with each siRNA. Because modified LC3 (LC3-II), a hallmark of autophagy, is degraded on achievement of autophagy, the levels of LC3-II were examined in the presence of protease inhibitors pepstatin A and E64d (Fig. 3*C*). Under physiological conditions, the LC3-II levels were higher in cells treated with NLRC4 or NLRP4 siRNA relative to those with control siRNA, suggesting that the autophagic process is constitutively promoted in the cells depleted of NLRC4 or NLRP4 (Fig. 3*C*). Following invasive GAS infection, the LC3-II levels were increased in all samples, but they were greater in NLRC4- or NLRP4-knockdown cells compared with control cells (Fig. 3*C*). The influence of decreased NLRC4 or NLRP4 on autophagy was also examined with well-known autophagy inducers, such as rapamycin, VSV, and other invasive bacteria (*L. monocytogenes*) (Supplemental Fig. 6*A–C*) (18). The treatment of rapamycin or VSV infection resulted in LC3-II accumulation in NLRC4- or NLRP4-knockdown cells at a level comparable to control cells (Supplemental Fig. 6*A*, 6*B*). In contrast, *L. monocytogenes* infection resulted in the enhancement of LC3-II accumulation by the knockdown of NLRC4 or NLRP4 (Supplemental Fig. 6*C*). Collectively, the data suggested that NLRC4 or NLRP4 negatively regulates the induction of autophagy upon invasive bacterial infection (Supplemental Fig. 6*A–C*).

To further confirm the influence of NLRC4 and NLRP4 on the autophagic process, the LC3-II levels were also monitored in the absence of protease inhibitors (Fig. 3*D*). Of interest, LC3-II was barely detected in NLRP4-knockdown cells under physiological conditions and even after GAS infection (Fig. 3*D*). The levels of the other hallmark of autophagy, p62, were lower in NLRP4 knockdown cells compared with control cells before GAS infection (Fig. 3*D*). The GAS infection did not affect the levels of p62 in the cells treated with siRNA of control, NLRC4-knockdown, or NLRP4-knockdown cells, indicating that phys-

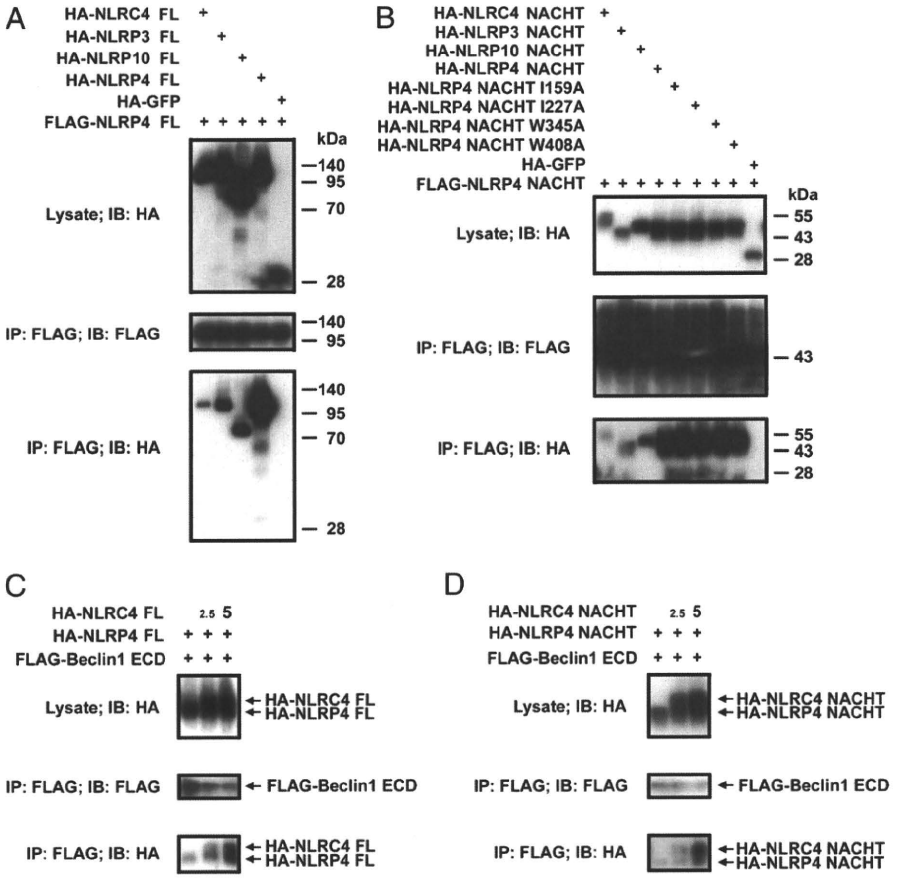


**FIGURE 2.** NACHT domains of NLRs are important for their oligomerization, as well as association with Beclin1. *A–D*, HEK293 cells were transfected with the indicated plasmids. Forty-eight hours posttransfection, the cells were subjected to immunoprecipitation and immunoblotting analysis. Representative results from at least three independent experiments are shown.

iological autophagy might be distinct from GAS-mediated autophagy on discrimination of substrates to degrade (Fig. 3*D*). In addition, the fluorescent microscopy analysis showed that the reduced NLRP4 resulted in greater numbers of LC3-II vacuoles under physiological conditions (Supplemental Fig. 7). These results collectively suggested that NLRC4 and NLRP4 negatively regulate the autophagic process under physiological conditions, as well as postinvasive bacterial infection, and that NLRP4, but not NLRC4, inhibits the protein-degradation process mediated by autophagy.

To examine whether the autophagic process regulated by NLRC4 or NLRP4 controls the intracellular bactericidal activity, the survival rate of intracellular bacteria was monitored following GAS infection (Fig. 3*E*). The number of bacteria that survived was significantly less in the NLRC4- or NLRP4-knockdown cells compared with control cells. Furthermore, the bacterial number was significantly less in the NLRP4-knockdown cells compared with the NLRC4-knockdown cells. Collectively, these data suggested that NLRC4 and NLRP4 negatively control the intracellular bactericidal activity, at least in part, through inhibition of the autophagic process (Fig. 3*E*).

We further investigated whether NLRP4 also functions as a negative regulator of autophagy in human primary cells, such as HUVECs. As shown in Fig. 3*F*, the knockdown of NLRP4 or NLRC4 in HUVECs resulted in accelerated autophagy after GAS infection. In addition, the reduction of NLRP4 resulted in greater bactericidal activity, suggesting that NLRP4 and NLRC4 are negative regulators of bactericide in HUVECs (Fig. 3*G*).

Some NLRs, such as NLRP3 and NLRC4, were shown to mediate the signaling leading to inflammasome activation. The secretion of IL-1β, a hallmark of inflammasome activation, was not detected in HeLa cells, even after treatment with a known inflammasome-activating agent, such as LPS, or GAS infection (Supplemental Fig. 8). Instead, the role of NLRP4 in inflammasome activation was examined by coexpression of inflammasome components: caspase-1 and apoptosis-associated speck-like protein containing a caspase recruitment domain. Coexpression of these molecules facilitated IL-1β secretion. The level of IL-1β was further increased in the presence of NLRC4 but not NLRP4, suggesting that NLRC4 is engaged, at least in part, in inflammasome activation in HeLa cells (Supplemental Fig. 8*B*).

### *NLRP4 is transiently recruited to bacteria-containing autophagosomes and dissociates from Beclin1 at an early stage of GAS infection*

To examine whether NLRP4 controls GAS-mediated autophagosome formation, the numbers of LC3 puncta were evaluated by confocal microscopy analysis (Fig. 4*A*, 4*B*, Supplemental Fig. 9*A*). As a result, the number of GAS-associated LC3$^+$ vacuoles was greater in NLRP4-knockdown cells than in control cells, suggesting that NLRP4 negatively regulates the induction of GAS-associated LC3 vacuoles (Fig. 4*A*, 4*B*, Supplemental Fig. 9*A*). To examine the subcellular dynamics of NLRP4 upon GAS infection, HeLa cells stably expressing CFP-NLRP4 and GFP-LC3 were established. Although diffusely present in the cytoplasm under physiological conditions, NLRP4 was recruited to the subplasma membrane area close to phagosomes containing GAS 30 min postinfection (Fig. 4*C*, Supplemental Fig. 9*B*). Similar relocalization was observed when the well-characterized phagosomal marker p57, also known as TACO or coronin1, was examined (Fig. 4*D*). In contrast, NLRP4 returned to a diffuse distribution in the cytoplasm 120 min postinfection, when most bacteria were

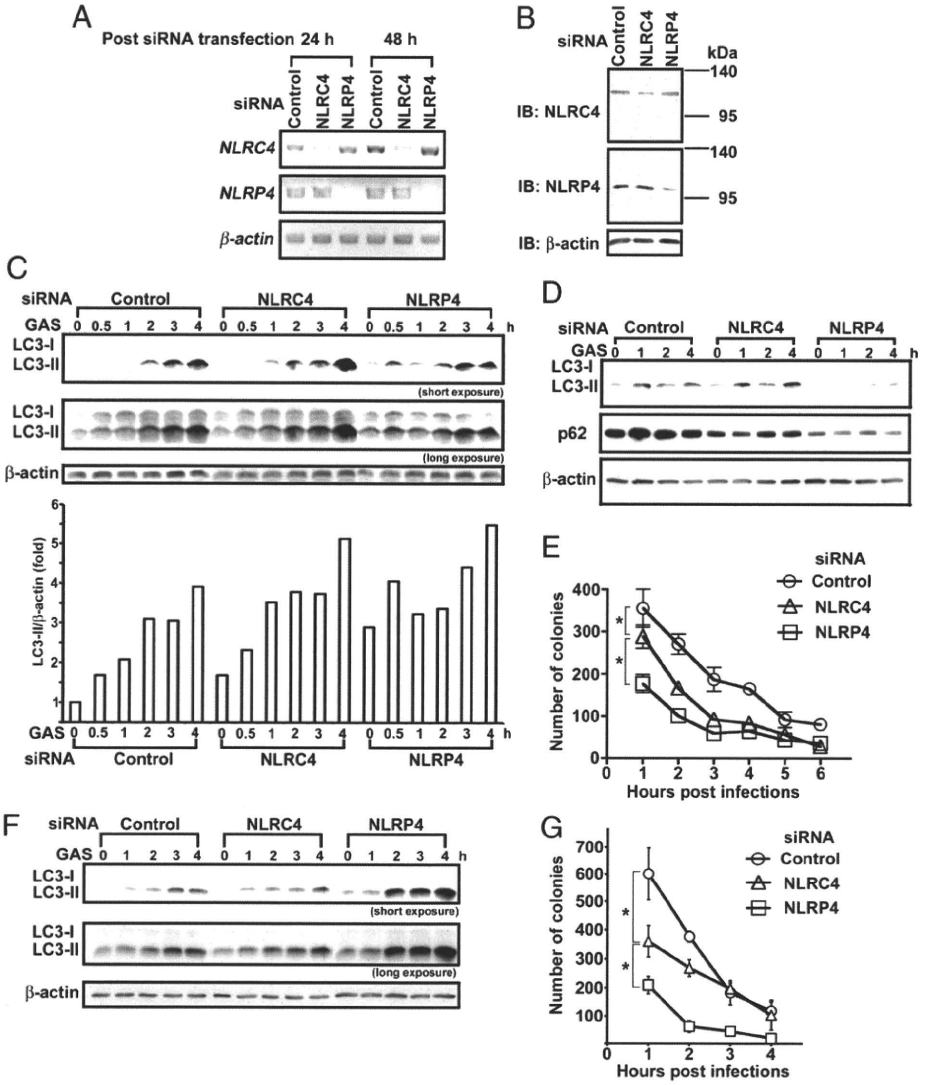


**FIGURE 3.** Enhancement of autophagy by repressing expression of NLRC4 or NLRP4. *A–C*, HeLa cells were transfected with control dsRNA or pooled dsRNAs targeting NLRC4 or NLRP4. *A*, Twenty-four or forty-eight hours following transfection, the mRNA levels of NLRC4, NLRP4, or β-actin were examined by RT-PCR analysis. *B*, Forty-eight hours following transfection, the protein levels of NLRC4, NLRP4, or β-actin were examined by immunoblotting. *C*, HeLa cells pretreated with siRNA were treated with protease inhibitors for 4 h and then were infected with GAS at an MOI of 50 for the indicated times. The levels of LC3-II in each sample were examined by immunoblotting analysis (*upper panel*). Band intensity was measured by Image J software. The intensity values of LC3-II were normalized to those of β-actin (*lower panel*). *D*, Cells pretreated with siRNA were infected with GAS at an MOI of 50 for the indicated times. The levels of LC3-II and p62 in each sample were examined by immunoblotting analysis. *E*, The HeLa cells were lysed in 1 ml of sterile distilled water, and 100 μl of each lysate was spread on THY agar plates ($n = 3$). The numbers of colonies were counted 24 h after incubation at 37°C. The graph shows the mean ± SD. Representative results from at least three independent experiments are shown. *F* and *G*, HUVECs pretreated with siRNA were further treated with protease inhibitors for 4 h and then infected with GAS at an MOI of 50 for the indicated times. *F*, The levels of LC3-II in each sample were examined by immunoblotting analysis. *G*, The HUVECs were lysed in 1 ml of sterile distilled water, and 100 μl of each lysate was spread on THY agar plates ($n = 3$). The numbers of colony were counted 24 h after plating. The graph shows the mean ± SD. Representative results from at least three independent experiments are shown. $^*p < 0.05$.

encapsulated by the $LC3^+$ vacuoles (i.e., autophagosomes) (Fig. 4*C*, Supplemental Fig. 9*B*). p57 remained localized in the vacuoles containing bacteria 120 min postinfection (Fig. 4*D*). We also evaluated whether the levels of interaction between NLRP4 and Beclin1 changed following GAS infection. HeLa cells were transfected with an expression plasmid encoding HA-NLRP4, and we found that HA-NLRP4 specifically interacted with endogenous Beclin1 (Fig. 4*E*). The level of interaction between HA-NLRP4 and Beclin1 decreased 60 min following GAS infection, but it returned to normal levels after 120 min (Fig. 4*E*). Because the size of Beclin1 is similar to that of an IgG H chain, the exact levels of immunoprecipitated Beclin1 could not be evaluated (Fig. 4*E*). We also found that the degrees of interaction between FLAG-NLRP4 and HA-Beclin1 decreased 30–60 min after GAS infection but returned to their original levels after 120 min (Fig. 4*F*). It was proposed that NLRP4 can detect infection by invasive bacteria, is recruited to the phagosomes, and dissociates from Beclin1, thereby permitting induction of autophagy, culminating in the induction of the intracellular bactericidal process.

### *NLRP4 but not NLRC4 inhibits maturation of autophagosomes*

Once the autophagosome undergoes maturation and couples with lysosomes, it functions as the autolysosome, initiating the intra-

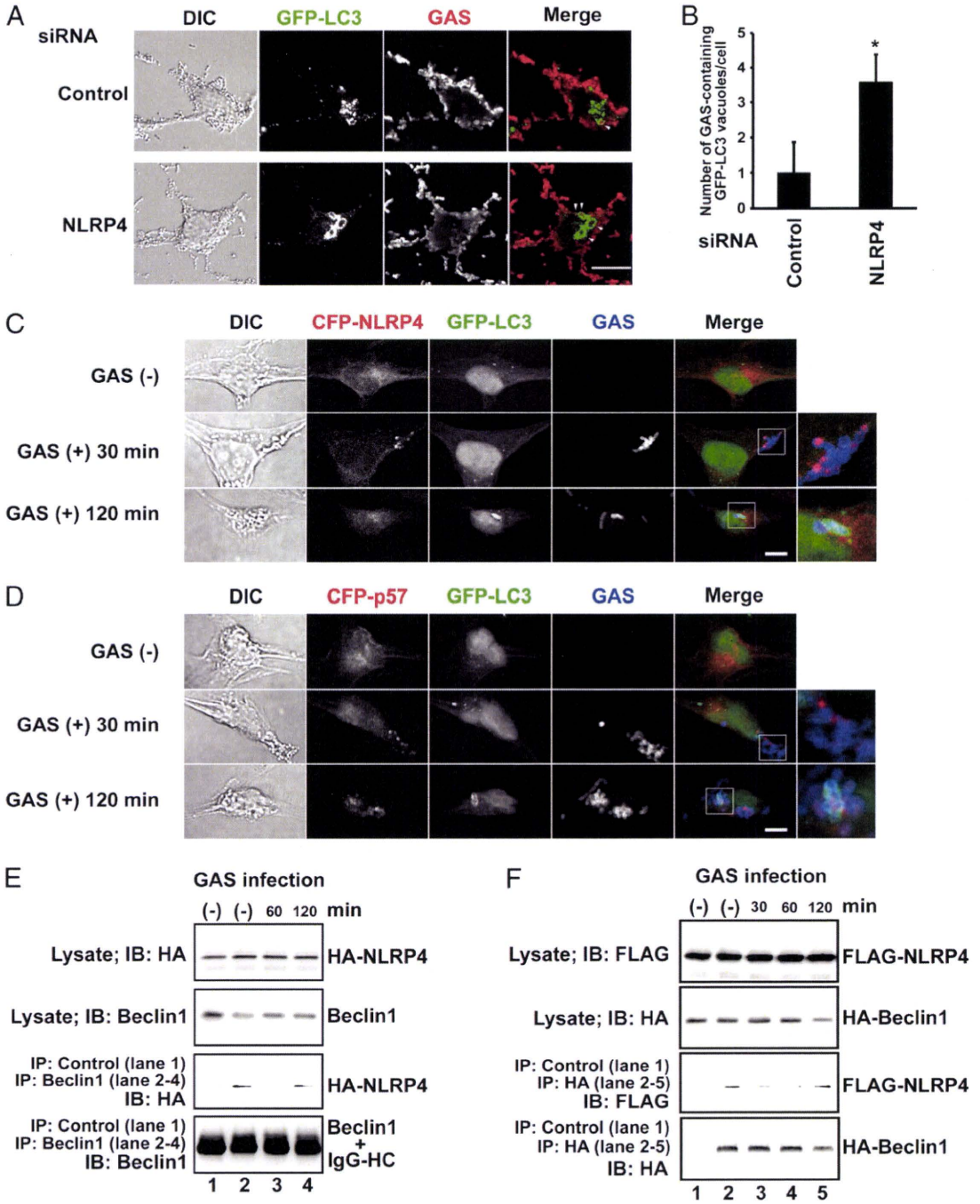


**FIGURE 4.** The dynamics of subcellular localization of NLRP4 and the levels of interaction between NLRP4 and Beclin1 following GAS infection. *A* and *B*, HeLa cells were cotransfected with the indicated siRNA and GFP-LC3 expression plasmid, and the cells were infected with GAS at an MOI of 100. At 2 h postinfection with GAS, the cells were fixed and immunostained with anti-GAS Ab, followed by Alexa 546-conjugated anti-rabbit Ab. The samples were subjected to confocal microscopy analysis. *A*, Representative photomicrographs from seven cells examined. Arrowheads in merge images denote GAS-associated LC3 vacuoles. Scale bar, 20 μm. *B*, The number of GAS-associated LC3 vacuoles (>2 μm) in individual cells was counted ($n = 15$). The graph shows the mean ± SD. *$p < 0.01$. HeLa cells stably expressing GFP-LC3 plus CFP-NLRP4 (*C*) or CFP-p57 (*D*) were infected with GAS at an MOI of 50 for the indicated times and then fixed. Intracellular GAS was immunostained with anti-GAS Ab, followed by Alexa Fluor 546-conjugated anti-rabbit Ab. The samples were examined under a confocal microscope. Scale bar, 20 μm. Representative photomicrographs from 10–15 cells examined. Three independent experiments gave similar results. HeLa cells were transfected with an expression plasmid for HA-NLRP4 (*E*) or FLAG-NLRP4 and HA-Beclin1 (*F*). Forty-eight hours after transfection, the cells were infected with GAS at an MOI of 50 for the indicated times. The cells were then subjected to immunoprecipitation assays. Representative results from at least three independent experiments are shown.

cellular bactericidal process. To monitor the real-time formation of autophagosomes and autolysosomes, we established a HeLa cell line that stably expressed the mRFP-GFP-LC3 fusion protein. According to a previous report (23), when this indicator protein is present in the autophagosome, the mixed fluorescence of red and green is detected as yellow. By contrast, in the autolysosome, the tertiary structure of GFP, but not that of mRFP, is disrupted because of low pH, and the indicator fluorescence is red.

Rab7, a small GTPase known to localize on the lysosome membrane, was recruited to the red fluorescent vacuoles but not to the yellow ones (data not shown). Using this indicator, we evaluated the maturation of the autophagosomes in living cells. The number of yellow vesicles was greater in NLRC4- and NLRP4-knockdown cells relative to control cells, suggesting that autophagosome formation is upregulated (Fig. 5*A*). By contrast, the number of red vesicles was significantly greater in NLRP4-knockdown cells compared with NLRC4-knockdown or control cells, indicating that the rate of autophagosome maturation is enhanced by interrupting NLRP4 expression but not NLRC4 expression (Fig. 5*A*, 5*B*). When these cells were infected with GAS, the number of yellow vesicles increased in NLRC4-knockdown cells compared with NLRP4-knockdown or control cells. Knockdown of NLRP4 seemed to accelerate the rate of autophagosome maturation, resulting in a reduction in the transient number of autophagosomes (Fig. 5*B*, 5*C*). Altogether, these results indicated that NLRC4 and NLRP4 negatively regulated the initiation of the autophagic process, whereas NLRP4, but not NLRC4, inhibited autophagosome maturation (Fig. 5*D*).

A recent study revealed that Rubicon, a negative regulator of the autophagic machinery, contains a property that is inhibitory for autophagosomal maturation because of a mechanism shared by the endosomal-maturation process, which is critically involved in EGF-dependent degradation of the EGFR. To examine whether NLRP4 has a similar property, the efficiency of EGFR degradation induced by EGF treatment was monitored by immunoblotting. As shown in Fig. 5*E*, the levels of EGFR were reduced in response to EGF treatment of HeLa cells. However, the rate of EGFR degradation was significantly greater in NLRP4-knockdown cells compared with NLRC4-knockdown or control cells. A similar result was obtained when the rate of EGFR degradation was examined using A549 cells (Supplemental Fig. 10). The formation of the autolysosome and endolysosome is mediated by the molecular mechanisms controlling tethering and fusion of vacuolar membranes. Such membrane dynamics are chiefly controlled by the C-VPS complex consisting of VPS11, VPS16, VPS18, and a small GTPase (Rab7) on the Rab5-labeled early endosomes. To examine the molecular mechanisms underlying NLRP4-mediated suppression of autophagosome maturation, the interaction between each C-VPS component and NLR family member was analyzed by immunoprecipitation (Fig. 5*F*). Significant levels of VPS11, VPS16, and VPS18 coprecipitated with NLRP4 compared with NLRC4 or control GFP, suggesting that NLRP4 has a stronger affinity for the C-VPS complex and, thereby, controlled the maturation process of the autophagosome and endosome (Fig. 5*F*).

## Discussion

This study elucidated that the NACHT domain of NLRs physically interacts with the ECD of Beclin1 and inhibits induction of the autophagic process. It was shown that Bcl-2 interacts with the Beclin1 BD (24), whereas UVRAG targets the Beclin1 CCD (7). CCD and ECD of Beclin1 are required for its interaction with PI3KC3 and a heterodimer of VPS34/VPS15 (7). However, molecular mechanisms underlying the complex formation of these Beclin1-interacting molecules and their cooperation or competition for the induction of autophagy are largely unknown. Results from our immunoprecipitation assay and gel-filtration analysis indicated that NLRP4 is a component of the 500–700-kDa cytoplasmic complex that contains Beclin1 (Fig. 1*C*, 1*F*). Previous studies and our present data showed that, under physiological conditions, the majority of cellular Beclin1 (52 kDa) complexes with VPS34 (100 kDa) and VPS15 (150 kDa) and that Beclin1 migrate into fractions spanning a relatively broad range of sizes

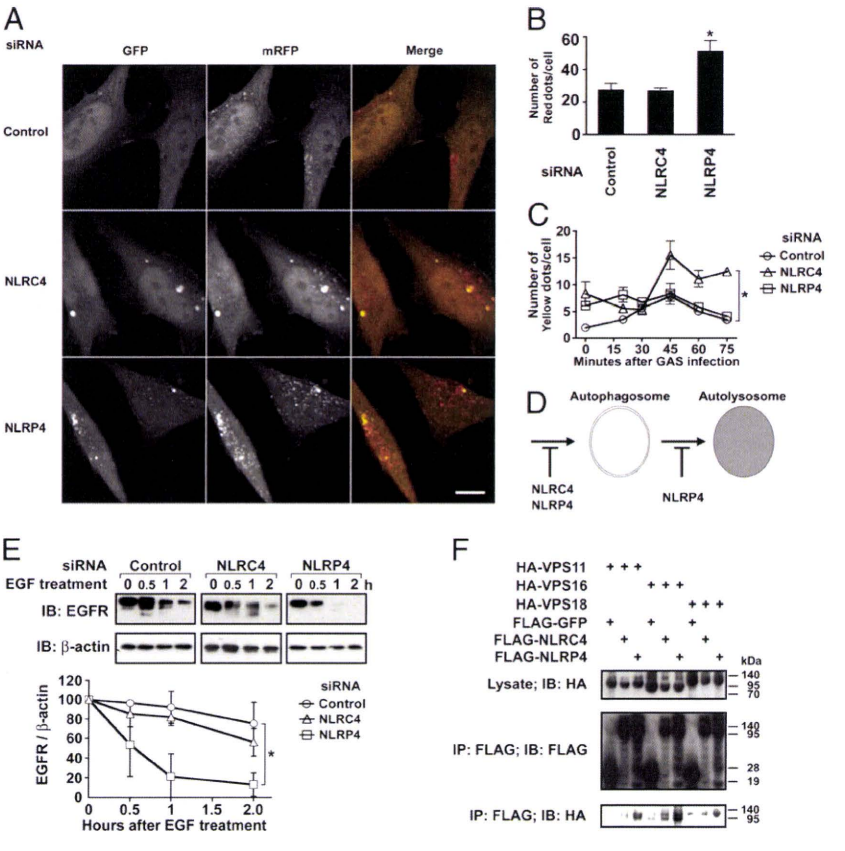


**FIGURE 5.** NLRP4 controls the maturation of autophagosome and endosome through the association with class C VPS. *A–C*, HeLa cells stably expressing mRFP-GFP-LC3 were transfected with control dsRNA or pooled dsRNAs targeting NLRC4 or NLRP4. *A* and *B*, Forty-eight hours following transfection, the cells were fixed and then analyzed under a confocal microscope. *A*, Representative photomicrographs are shown; scale bar, 20 μm. *B*, The number of red fluorescent dots (>1 μm) in individual cells was counted ($n$ = 10). The graph shows the mean ± SD. *C*, Forty-eight hours after transfection, the cells were infected with GAS at an MOI of 50 for the indicated times, fixed, and analyzed under a confocal microscope. The number of yellow fluorescent dots (>1 μm) in individual cells was counted ($n$ = 10). The graph shows the mean ± SD. *D*, A schematic diagram of target step(s) by NLRC4 or NLRP4 in the course of autophagic flux. *E*, HeLa cells were transfected with control dsRNA or pooled dsRNAs targeting NLRC4 or NLRP4. Forty-eight hours posttransfection, the cells were treated with EGF (200 ng/ml) for the indicated times. The levels of EGFR degradation were examined by immunoblotting analysis. Representative results of at least three independent experiments are shown. The graph shows the mean ± SD. *F*, HEK293 cells were transfected with the indicated plasmids. Forty-eight hours after transfection, the cells were subjected to immunoprecipitation and immunoblotting analyses. Representative results of at least three independent experiments are shown. *$p < 0.05$.

(400–700 kDa). Thus, it was suggested that the Beclin1–PI3KC3 complex (~300 kDa) further interacts with other molecules of different sizes. A recent study revealed that the Atg14L–Beclin1–PI3KC3 complex is required for autophagosome formation, whereas the UVRAG–Beclin1–PI3KC3 complex is crucial for maturation of the autophagosome and endosome. Further interaction of Rubicon with the UVRAG–Beclin1–PI3KC3 complex inhibited the maturation process for the autophagosome and endosome (8). Accordingly, the dynamics of Atg14L, which localizes to the endoplasmic reticulum, isolation membrane, and autophagosome, are different from those of UVRAG and Rubicon, which are present in the endosome and lysosome. Therefore, it was suggested that various types of the Beclin1-containing complex are organized in response to the cellular environment, resulting in the control of autophagic flux, whereas interaction with Rubicon inhibits autophagic flux. Although the present study revealed that NLRP4 is one component of the Beclin1 complex, further studies are required to elucidate which factors control the formation of the NLRP4–Beclin1 complex to negatively regulate autophagy during invasive bacterial infection.

Previous studies characterized the nature of GAS-containing autophagosome-like vacuoles (GcAVs). GcAVs are large (>10 μm) relative to physiological autophagosomes (0.5–1.0 μm) (4). Although GcAVs were shown to be $LC3^+$ and are generated in an Atg5-dependent manner, a recent study suggested that Rab7 recruitment to GcAVs, but not physiological autophagosomes, plays an important role in the formation of GcAVs that is required for elimination of invasive GAS bacteria (25). Because our data showed that the knockdown of NLRP4 increased the number of GcAVs and that NLRP4 interacted with the components of the C-VPS complex linking Rab7 activation, it was strongly suggested that NLRP4 correlates with the activation of Rab7 on GcAVs (Figs. 4*A*, 4*B*, 5*F*).

Several studies investigated the cellular functions of NLRP4, but none of them revealed its biological role associated with bacterial infection (26–28). Another interesting aspect of NLRP4 that we elucidated in this study was the subcellular dynamics of this molecule in response to bacterial infection (i.e., NLRP4 is recruited and accumulated on bacteria-containing phagosomes at an early stage of infection). Previous studies demonstrated that mice deficient for NLRC4 or NLRP3 have defective IL-1β production in response to bacterial components, such as flagellin or LPS. There are no reports showing evidence of the direct interaction between NLRs and bacterial components, although several members of the NLR family were shown to be linked to the bacterial-recognition mechanism (29). Furthermore, it was recently shown that NOD1 and NOD2, the NLR sensors of bacterial peptidoglycan (muramyldipeptide), directly induce autophagy by recruiting Atg16L1 to the phagosomes containing bacteria (30, 31). Accompanying these findings, recent genome-wide association studies revealed that the loss-of-function mutation of the *Atg16l1* gene, as well as the gain-of-function mutation of the *Nod2* gene, are seen at significantly greater rates in patients with Crohn's disease, suggesting that the NLR sensors and autophagy are associated with the pathogenesis of inflammation caused by bacteria (32, 33). The epithelial cell-expressing Atg16L1 T300A mutant, a risk variant of Crohn's disease, undergoes physiological autophagy but is defective for the autophagic process induced by bacterial infection. This would indicate that Atg16L mediates a specific signaling pathway linking bacterial recognition and the initiation of autophagy (34). In fact, a previous study revealed that Atg16L1-deficient murine cells are more susceptible to secreting IL-1β in response to inflammatory stimuli, such as LPS or dextran sulfate sodium (35). Because Atg16L was shown to be an essential factor in the regulation of autophagy downstream of Beclin1-mediated signaling, it was suggested that Atg16L–NOD2 interaction is a crossroad between macroautophagy and inflammasome activation. Because our research also clarified the novel molecular interaction between NLRP4 and Beclin1, we are investigating, in on-going studies, upstream signaling events regulating the association between inflammasome and autophagy.

With regard to autophagy-inducing pathways specific to bacterial infection, it was shown that signaling mediated by TLRs can lead to autophagosome formation (36, 37). Immunity-related p47 guanosine triphosphatase M, a cytoplasmic molecule crucial in the recognition and elimination of invasive pathogens, also mediates the induction of autophagy following *Mycobacterium tuberculosis* infection (38, 39). Several studies have begun to elucidate the mechanisms underlying the pathway linking the sensory machinery of pathogens and the initiation of autophagy. Further genetic studies would determine how NLRP4, directly or indirectly, contributes to the autophagic bactericidal process during invasive bacterial infections and whether NLRP4 regulates inflammasome activation upon invasive bacterial infection with or without other NLR members.

## Acknowledgments

We thank Drs. E. Hanski (The Hebrew University-Hadassah Medical School) and H. Miyoshi (RIKEN BioResource Center, Tsukuba, Japan) for providing experimental materials and suggestions and N. Araya for technical assistance.

## Disclosures

The authors have no financial conflicts of interest.

## References

1. Kuma, A., M. Hatano, M. Matsui, A. Yamamoto, H. Nakaya, T. Yoshimori, Y. Ohsumi, T. Tokuhisa, and N. Mizushima. 2004. The role of autophagy during the early neonatal starvation period. *Nature* 432: 1032–1036.
2. Komatsu, M., S. Waguri, T. Ueno, J. Iwata, S. Murata, I. Tanida, J. Ezaki, N. Mizushima, Y. Ohsumi, Y. Uchiyama, et al. 2005. Impairment of starvation-induced and constitutive autophagy in Atg7-deficient mice. *J. Cell Biol.* 169: 425–434.
3. Nishida, Y., S. Arakawa, K. Fujitani, H. Yamaguchi, T. Mizuta, T. Kanaseki, M. Komatsu, K. Otsu, Y. Tsujimoto, and S. Shimizu. 2009. Discovery of Atg5/Atg7-independent alternative macroautophagy. *Nature* 461: 654–658.
4. Nakagawa, I., A. Amano, N. Mizushima, A. Yamamoto, H. Yamaguchi, T. Kamimoto, A. Nara, J. Funao, M. Nakata, K. Tsuda, et al. 2004. Autophagy defends cells against invading group A *Streptococcus*. *Science* 306: 1037–1040.
5. Birmingham, C. L., V. Canadien, E. Gouin, E. B. Troy, T. Yoshimori, P. Cossart, D. E. Higgins, and J. H. Brumell. 2007. *Listeria monocytogenes* evades killing by autophagy during colonization of host cells. *Autophagy* 3: 442–451.
6. Yoshimori, T., and T. Noda. 2008. Toward unraveling membrane biogenesis in mammalian autophagy. *Curr. Opin. Cell Biol.* 20: 401–407.
7. Liang, C., P. Feng, B. Ku, I. Dotan, D. Canaani, B. H. Oh, and J. U. Jung. 2006. Autophagic and tumour suppressor activity of a novel Beclin1-binding protein UVRAG. *Nat. Cell Biol.* 8: 688–699.
8. Matsunaga, K., T. Saitoh, K. Tabata, H. Omori, T. Satoh, N. Kurotori, I. Maejima, K. Shirahama-Noda, T. Ichimura, T. Isobe, et al. 2009. Two Beclin 1-binding proteins, Atg14L and Rubicon, reciprocally regulate autophagy at different stages. *Nat. Cell Biol.* 11: 385–396.
9. Zhong, Y., Q. J. Wang, X. Li, Y. Yan, J. M. Backer, B. T. Chait, N. Heintz, and Z. Yue. 2009. Distinct regulation of autophagic activity by Atg14L and Rubicon associated with Beclin 1-phosphatidylinositol-3-kinase complex. *Nat. Cell Biol.* 11: 468–476.
10. Liang, C., J. S. Lee, K. S. Inn, M. U. Gack, Q. Li, E. A. Roberts, I. Vergne, V. Deretic, P. Feng, C. Akazawa, and J. U. Jung. 2008. Beclin1-binding UVRAG targets the class C Vps complex to coordinate autophagosome maturation and endocytic trafficking. *Nat. Cell Biol.* 10: 776–787.
11. Wilmanski, J. M., T. Petnicki-Ocwieja, and K. S. Kobayashi. 2008. NLR proteins: integral members of innate immunity and mediators of inflammatory diseases. *J. Leukoc. Biol.* 83: 13–30.
12. Suzuki, T., L. Franchi, C. Toma, H. Ashida, M. Ogawa, Y. Yoshikawa, H. Mimuro, N. Inohara, C. Sasakawa, and G. Nuñez. 2007. Differential regulation of caspase-1 activation, pyroptosis, and autophagy via Ipaf and ASC in *Shigella*-infected macrophages. *PLoS Pathog.* 3: e111.
13. Kobiyama, K., F. Takeshita, N. Jounai, A. Sakaue-Sawano, A. Miyawaki, K. J. Ishii, T. Kawai, S. Sasaki, H. Hirano, N. Ishii, et al. 2010. Extrachromosomal

histone H2B mediates innate antiviral immune responses induced by intracellular double-stranded DNA. *J. Virol.* 84: 822–832.
14. Martinon, F., K. Burns, and J. Tschopp. 2002. The inflammasome: a molecular platform triggering activation of inflammatory caspases and processing of proIL-beta. *Mol. Cell* 10: 417–426.
15. Takeshita, F., K. J. Ishii, K. Kobiyama, Y. Kojima, C. Coban, S. Sasaki, N. Ishii, D. M. Klinman, K. Okuda, S. Akira, and K. Suzuki. 2005. TRAF4 acts as a silencer in TLR-mediated signaling through the association with TRAF6 and TRIF. *Eur. J. Immunol.* 35: 2477–2485.
16. Miyoshi, H., U. Blömer, M. Takahashi, F. H. Gage, and I. M. Verma. 1998. Development of a self-inactivating lentivirus vector. *J. Virol.* 72: 8150–8157.
17. Miyoshi, H., M. Takahashi, F. H. Gage, and I. M. Verma. 1997. Stable and efficient gene transfer into the retina using an HIV-based lentiviral vector. *Proc. Natl. Acad. Sci. USA* 94: 10319–10323.
18. Jounai, N., F. Takeshita, K. Kobiyama, A. Sawano, A. Miyawaki, K. Q. Xin, K. J. Ishii, T. Kawai, S. Akira, K. Suzuki, and K. Okuda. 2007. The Atg5 Atg12 conjugate associates with innate antiviral immune responses. *Proc. Natl. Acad. Sci. USA* 104: 14050–14055.
19. Takeshita, F., K. Suzuki, S. Sasaki, N. Ishii, D. M. Klinman, and K. J. Ishii. 2004. Transcriptional regulation of the human TLR9 gene. *J. Immunol.* 173: 2552–2561.
20. Sakaue-Sawano, A., H. Kurokawa, T. Morimura, A. Hanyu, H. Hama, H. Osawa, S. Kashiwagi, K. Fukami, T. Miyata, H. Miyoshi, et al. 2008. Visualizing spatiotemporal dynamics of multicellular cell-cycle progression. *Cell* 132: 487–498.
21. Geddes, B. J., L. Wang, W. J. Huang, M. Lavellee, G. A. Manji, M. Brown, M. Jurman, J. Cao, J. Morgenstern, S. Merriam, et al. 2001. Human CARD12 is a novel CED4/Apaf-1 family member that induces apoptosis. *Biochem. Biophys. Res. Commun.* 284: 77–82.
22. Komatsu, M., S. Waguri, M. Koike, Y. S. Sou, T. Ueno, T. Hara, N. Mizushima, J. Iwata, J. Ezaki, S. Murata, et al. 2007. Homeostatic levels of p62 control cytoplasmic inclusion body formation in autophagy-deficient mice. *Cell* 131: 1149–1163.
23. Kimura, S., N. Fujita, T. Noda, and T. Yoshimori. 2009. Monitoring autophagy in mammalian cultured cells through the dynamics of LC3. *Methods Enzymol.* 452: 1–12.
24. Pattingre, S., A. Tassa, X. Qu, R. Garuti, X. H. Liang, N. Mizushima, M. Packer, M. D. Schneider, and B. Levine. 2005. Bcl-2 antiapoptotic proteins inhibit Beclin 1-dependent autophagy. *Cell* 122: 927–939.
25. Yamaguchi, H., I. Nakagawa, A. Yamamoto, A. Amano, T. Noda, and T. Yoshimori. 2009. An initial step of GAS-containing autophagosome-like vacuoles formation requires Rab7. *PLoS Pathog.* 5: e1000670.
26. Grenier, J. M., L. Wang, G. A. Manji, W. J. Huang, A. Al-Garawi, R. Kelly, A. Carlson, S. Merriam, J. M. Lora, M. Briskin, et al. 2002. Functional screening of five PYPAF family members identifies PYPAF5 as a novel regulator of NF-kappaB and caspase-1. *FEBS Lett.* 530: 73–78.
27. Fiorentino, L., C. Stehlik, V. Oliveira, M. E. Ariza, A. Godzik, and J. C. Reed. 2002. A novel PAAD-containing protein that modulates NF-kappa B induction by cytokines tumor necrosis factor-alpha and interleukin-1beta. *J. Biol. Chem.* 277: 35333–35340.
28. Zhang, P., M. Dixon, M. Zucchelli, F. Hambiliki, L. Levkov, O. Hovatta, and J. Kere. 2008. Expression analysis of the NLRP gene family suggests a role in human preimplantation development. *PLoS ONE* 3: e2755.
29. Hise, A. G., J. Tomalka, S. Ganesan, K. Patel, B. A. Hall, G. D. Brown, and K. A. Fitzgerald. 2009. An essential role for the NLRP3 inflammasome in host defense against the human fungal pathogen *Candida albicans*. *Cell Host Microbe* 5: 487–497.
30. Travassos, L. H., L. A. Carneiro, M. Ramjeet, S. Hussey, Y. G. Kim, J. G. Magalhaes, L. Yuan, F. Soares, E. Chea, L. Le Bourhis, et al. 2010. Nod1 and Nod2 direct autophagy by recruiting ATG16L1 to the plasma membrane at the site of bacterial entry. *Nat. Immunol.* 11: 55–62.
31. Cooney, R., J. Baker, O. Brain, B. Danis, T. Pichulik, P. Allan, D. J. Ferguson, B. J. Campbell, D. Jewell, and A. Simmons. 2010. NOD2 stimulation induces autophagy in dendritic cells influencing bacterial handling and antigen presentation. *Nat. Med.* 16: 90–97.
32. Abbott, D. W., A. Wilkins, J. M. Asara, and L. C. Cantley. 2004. The Crohn's disease protein, NOD2, requires RIP2 in order to induce ubiquitinylation of a novel site on NEMO. *Curr. Biol.* 14: 2217–2227.
33. Hampe, J., A. Franke, P. Rosenstiel, A. Till, M. Teuber, K. Huse, M. Albrecht, G. Mayr, F. M. De La Vega, J. Briggs, et al. 2007. A genome-wide association scan of nonsynonymous SNPs identifies a susceptibility variant for Crohn disease in ATG16L1. *Nat. Genet.* 39: 207–211.
34. Kuballa, P., A. Huett, J. D. Rioux, M. J. Daly, and R. J. Xavier. 2008. Impaired autophagy of an intracellular pathogen induced by a Crohn's disease associated ATG16L1 variant. *PLoS ONE* 3: e3391.
35. Saitoh, T., N. Fujita, M. H. Jang, S. Uematsu, B. G. Yang, T. Satoh, H. Omori, T. Noda, N. Yamamoto, M. Komatsu, et al. 2008. Loss of the autophagy protein Atg16L1 enhances endotoxin-induced IL-1beta production. *Nature* 456: 264–268.
36. Delgado, M. A., R. A. Elmaoued, A. S. Davis, G. Kyei, and V. Deretic. 2008. Toll-like receptors control autophagy. *EMBO J.* 27: 1110–1121.
37. Xu, Y., C. Jagannath, X. D. Liu, A. Sharafkhaneh, K. E. Kolodziejska, and N. T. Eissa. 2007. Toll-like receptor 4 is a sensor for autophagy associated with innate immunity. *Immunity* 27: 135–144.
38. MacMicking, J. D., G. A. Taylor, and J. D. McKinney. 2003. Immune control of tuberculosis by IFN-gamma-inducible LRG-47. *Science* 302: 654–659.
39. Singh, S. B., A. S. Davis, G. A. Taylor, and V. Deretic. 2006. Human IRGM induces autophagy to eliminate intracellular mycobacteria. *Science* 313: 1438–1441.

Published April 27, 2011, doi:10.4049/jimmunol.1004036



# A New Subset of CD103$^+$CD8$\alpha^+$ Dendritic Cells in the Small Intestine Expresses TLR3, TLR7, and TLR9 and Induces Th1 Response and CTL Activity

Kosuke Fujimoto,*,†,1 Thangaraj Karuppuchamy,*,†,1 Naoki Takemura,*,† Masaki Shimohigoshi,*,† Tomohisa Machida,*,† Yasunari Haseda,‡,§ Taiki Aoshi,‡,§ Ken J. Ishii,‡,§ Shizuo Akira,*,† and Satoshi Uematsu*,†

**CD103$^+$ dendritic cells (DCs) are the major conventional DC population in the intestinal lamina propria (LP). Our previous report showed that a small number of cells in the LP could be classified into four subsets based on the difference in CD11c/CD11b expression patterns: CD11c$^{hi}$CD11b$^{lo}$ DCs, CD11c$^{hi}$CD11b$^{hi}$ DCs, CD11c$^{int}$CD11b$^{int}$ macrophages, and CD11c$^{int}$CD11b$^{hi}$ eosinophils. The CD11c$^{hi}$CD11b$^{hi}$ DCs, which are CD103$^+$, specifically express TLR5 and induce the differentiation of naive B cells into IgA$^+$ plasma cells. These DCs also mediate the differentiation of Ag-specific Th17 and Th1 cells in response to flagellin. We found that small intestine CD103$^+$ DCs of the LP (LPDCs) could be divided into a small subset of CD8$\alpha^+$ cells and a larger subset of CD8$\alpha^-$ cells. Flow cytometry analysis revealed that CD103$^+$CD8$\alpha^+$ and CD103$^+$CD8$\alpha^-$ LPDCs were equivalent to CD11c$^{hi}$ CD11b$^{lo}$ and CD11c$^{hi}$CD11b$^{hi}$ subsets, respectively. We analyzed a novel subset of CD8$\alpha^+$ LPDCs to elucidate their immunological function. CD103$^+$CD8$\alpha^+$ LPDCs expressed TLR3, TLR7, and TLR9 and produced IL-6 and IL-12p40, but not TNF-$\alpha$, IL-10, or IL-23, following TLR ligand stimulation. CD103$^+$CD8$\alpha^+$ LPDCs did not express the gene encoding retinoic acid-converting enzyme *Raldh2* and were not involved in T cell-independent IgA synthesis or Foxp3$^+$ regulatory T cell induction. Furthermore, CD103$^+$CD8$\alpha^+$ LPDCs induced Ag-specific IgG in serum, a Th1 response, and CTL activity in vivo. Accordingly, CD103$^+$CD8$\alpha^+$ LPDCs exhibit a different function from CD103$^+$CD8$\alpha^-$ LPDCs in active immunity. This is the first analysis, to our knowledge, of CD8$\alpha^+$ DCs in the LP of the small intestine.** *The Journal of Immunology*, **2011, 186: 000–000.**

The gastrointestinal tract is constantly exposed to food proteins and commensal bacteria. Although the intestinal immune system has evolved mechanisms that maintain immunological tolerance to food Ags and commensal organisms, it also recognizes invasive pathogens and induces appropriate protective immune responses to eliminate them. Dendritic cells (DCs) are thought to play a key role in discriminating between commensal microorganisms and potentially harmful pathogens and in maintaining the balance between tolerance and active immunity. DCs in the intestine are present not only in GALT, such as the Peyer's patches and isolated lymphoid follicles, but also in the lamina propria (LP) (1). CD103$^+$ DCs and CX3CR1$^+$ DCs are representative DCs in the intestinal LP (LPDCs). Recent reports have shown that CD103$^+$ LPDCs and CX3CR1$^+$ LPDCs are derived from two distinct DC lineages and that they serve separate immune functions in the intestine (2, 3). CX3CR1$^+$ DCs in the LP are known to penetrate epithelial tight junctions to sample luminal bacteria (4, 5). However, CX3CR1$^+$ DCs are nonmigratory and display poor T cell stimulatory capacity (6). However, CD103$^+$ DCs were shown to migrate from the LP to the mesenteric lymph nodes (MLNs) in a CCR7-dependent manner and to induce Foxp3$^+$ regulatory T cells (Tregs) via the dietary metabolite retinoic acid (RA) (7–10). RA-producing CD103$^+$ DCs in MLNs induce $\alpha4\beta_7$ integrin and CCR9 expression on naive lymphocytes to establish gut tropism (11). Previously, we reported that low-density cells in the LP could be classified into four subsets on the basis of their different CD11c/CD11b expression patterns: CD11c$^{hi}$CD11b$^{lo}$ DCs, CD11c$^{hi}$CD11b$^{hi}$ DCs, CD11c$^{int}$CD11b$^{int}$ macrophages, and CD11c$^{int}$CD11b$^{hi}$ eosinophils (12). The CD11c$^{hi}$CD11b$^{hi}$ subset, which is CD103$^+$, expresses TLR5 and TLR9 and produces proinflammatory cytokines such as IL-6 and IL-12 in response to flagellin and CpG oligodeoxynucleotide (ODN) (12, 13). The CD11c$^{hi}$CD11b$^{hi}$ subset specifically expresses mRNA of retinal dehydrogenase isoform 2 (Raldh2), which catalyzes the conversion of retinal to RA (12, 13). The ability to produce RA enables the CD11c$^{hi}$CD11b$^{hi}$ DC subset to induce a flagellin-mediated T cell-independent IgA class-switch recombination of B cells (12, 13). Furthermore, the CD11c$^{hi}$

*Laboratory of Host Defense, World Premier International Immunology Frontier Research Center, Osaka University, Osaka 565-0871, Japan; †Department of Host Defense, Research Institute for Microbial Diseases, Osaka University, Osaka 565-0871, Japan; ‡Laboratory of Adjuvant Innovation, National Institute of Biomedical Innovation, Osaka 567-0085, Japan; and §Laboratory of Vaccine Science, Osaka University, Osaka 565-0871, Japan

1K.F. and T.K. contributed equally to this work.

Received for publication December 10, 2010. Accepted for publication March 30, 2011.

This work was supported by a grant from the National Institutes of Health (PO1 AI070167 to S.A.), a Grant-in-Aid from the Ministry of Education, Culture, Sports, Science and Technology of Japan (to S.A.), a Grant-in-Aid for Specially Promoted Research, a Grant-in-Aid for Scientific Research on Priority Areas, and a Grant-in-Aid for Young Scientists (A) (to S.U.).

Address correspondence and reprint requests to Dr. Satoshi Uematsu, Laboratory of Host Defense, World Premier International Immunology Frontier Research Center, Osaka University, 3-1 Yamadaoka, Suita, Osaka 565-0851, Japan. E-mail address: uemattsu@biken.osaka-u.ac.jp

The online version of this article contains supplemental material.

Abbreviations used in this article: cDC, conventional dendritic cell; DC, dendritic cell; LP, lamina propria; LPDC, dendritic cell of the lamina propria; MLN, mesenteric lymph node; ODN, oligodeoxynucleotide; poly I:C, polyinosinic-polycytidylic acid; Raldh2, retinal dehydrogenase isoform 2; rhIL-2, recombinant human IL-2; RORγT, retinoic acid-related orphan receptor γT; Tg, transgenic; Treg, regulatory T cell.

CD11b$^{hi}$ subset promotes Th1 and Th17 cell differentiation in response to TLR ligands (12, 14).

We show that CD103$^+$ LPDCs in the small intestine are divided into a small subset of CD8α$^+$ cells and a larger subset of CD8α$^-$ cells. According to the flow cytometry analysis, CD103$^+$CD8α$^+$ and CD103$^+$CD8α$^-$ LPDCs were equivalent to CD11c$^{hi}$CD11b$^{lo}$ and CD11c$^{hi}$CD11b$^{hi}$ subsets, respectively. We analyzed the novel subset of CD8α$^+$ LPDCs to elucidate their immunological functions. The CD103$^+$CD8α$^+$ LPDCs expressed TLR3, TLR7, and TLR9 and produced IL-6 and IL-12p40 but not TNF-α, IL-10, or IL-23 in response to their respective TLR ligands. In contrast to CD103$^+$CD8α$^-$ LPDCs, CD103$^+$CD8α$^+$ LPDCs did not express the gene encoding the RA-converting enzyme, *Raldh2*, and were not involved in T cell-independent IgA synthesis and Foxp3$^+$ Treg induction. We further analyzed immunogenicity in Ag-loaded CD103$^+$CD8α$^+$ LPDCs in vivo. CD103$^+$CD8α$^+$ LPDCs induced Ag-specific IgG in serum, Th1 response, and CTL activity. In contrast, CD103$^+$CD8α$^-$ LPDCs induced Ag-specific IgG in serum as well as IgA in stool samples and also induced Th1 and Th17 responses and strong CTL activity. All of these results suggest that CD103$^+$CD8α$^+$ LPDCs have a different function to CD103$^+$CD8α$^-$ LPDCs in active immunity.

## Materials and Methods

### *Reagents*

Flagellin and CpG ODN (ODN1668) were purified as previously described (13). Polyinosinic-polycytidylic acid (poly I:C) and R-848 were purchased from Invivogen. Mouse MHC class I ($K^b$)-binding peptide $OVA_{257–264}$ (SIINFEKL) and MHC class II-binding $OVA_{323–339}$ (ISQAVHAAHAEINEAAGR) were obtained from Hokkaido System Science. Recombinant human TGF-β1 was purchased from R&D Systems.

### *Mice*

C57BL/6 mice were purchased from CLEA Japan. OT-I transgenic (Tg) mice and OT-II Tg mice (C57BL/6) were provided by W.R. Heath (Department of Microbiology and Immunology, University of Melbourne, Parkville, VIC, Australia) (12). All animal experiments were carried out with the approval of the Animal Research Committee of the Research Institute for Microbial Diseases at Osaka University.

### *Flow cytometry*

All Abs and reagents were obtained from BD Pharmingen unless otherwise stated. Before staining, FcRs were blocked for 15 min at 4°C. LPCs were stained with the following biotinylated mAbs: CD11b (M1/70), CD11c (HL3), CD103 (M290), and CD8α (53-6.7). Cocultured B cells or LP leukocytes were surface-stained with PerCP-Cy5.5–labeled anti-B220 (RA3-6B2). Cells were then fixed and permeabilized with Cytofix/Cytoperm and incubated with biotin-conjugated IgA (C10-1) followed by intracellular staining with allophycocyanin-labeled streptavidin. The surface of cocultured T cells was stained with PerCP-Cy5.5–labeled anti-CD4 (L3T4). Cells were then fixed and permeabilized with Cytofix/Cytoperm before intracellular staining with allophycocyanin-labeled anti-Foxp3 (FJK-16s; eBioscience) (Fig. 4), PE-labeled anti–IFN-γ (XMG1.2), allophycocyanin-labeled anti–IL-17 (TCC11-18H10.1) (Fig. 5*B*), PE-labeled anti–T-bet (4B10; eBioscience), or PE-labeled anti-retinoic acid-related orphan receptor γT (RORγT) (AFKJS-9; eBioscience) (Supplemental Fig. 1). Data were acquired with an FACSCalibur or FACSCanto II (BD Biosciences) and analyzed using the software FlowJo 8.6 (Tree Star).

### *Cells*

Small intestinal segments were treated with PBS containing 10% FCS, 20 mM HEPES, 100 U/ml penicillin, 100 μg/ml streptomycin, 1 mM sodium pyruvate, 10 mM EDTA, and 10 μg/ml polymyxin B (Calbiochem) for 30 min at 37°C to remove epithelial cells, followed by extensive washing with PBS. Small intestinal segments were digested with 400 Mandl units/ml collagenase D (Roche) and 10 μg/ml DNase I (Roche) in RPMI 1640/10% FCS with continuous stirring at 37°C for 45–90 min. EDTA was added (10 mM final concentration), and the cell suspension was incubated for an additional 5 min at 37°C. Cells were passed through a 17.5% Accudenz (Accurate Chemical & Scientific) solution to enrich the DCs. The obtained cells were incubated with FITC-conjugated anti-CD103, PE-conjugated anti-CD8α, PE-Cy7–conjugated anti-CD11c, and allophycocyanin-Cy7–conjugated anti-CD11b after FcR blocking. CD11c$^{hi}$ DC subsets were sorted on the basis of their expression of CD103 and CD8α using an FACSAria (BD Biosciences). The purity of the sorted DCs was routinely >95%. Naive CD4$^+$ T cells from the spleens of OT-II Tg mice were purified by magnetic sorting using mouse anti-CD4 beads (Miltenyi Biotec). Naive CD8$^+$ T cells from the spleens of OT-I Tg mice were purified by magnetic sorting using the CD8a$^+$ T Cell Isolation kit II (Miltenyi Biotec). Peritoneal cells from C57BL/6 mice were incubated with FITC-conjugated anti-IgD (11-26c.2a) and PE-Cy7–conjugated anti-IgM (R6-60.2; both BD Pharmingen) after FcR blocking. Naive B cells were sorted on the basis of their expression of IgD and IgM using an FACSAria system (BD Biosciences). The purity of the sorted cells was routinely >95%. EL-4 cells were obtained from American Type Culture Collection (TIB-39).

### *RT-PCR and quantitative real-time PCR*

RNA (1 μg) was reverse-transcribed using Superscript II Reverse Transcriptase (Invitrogen) according to the manufacturer's instructions with random hexamers as primers. The sequences of primers specific for *Tlr2*, *Tlr3*, *Tlr4*, *Tlr5*, *Tlr7*, *Tlr9*, or *Actb* have been described previously (12). The primer pairs and Taq polymerase (Takara Shuzo) were used for PCR as follows: 25 cycles at 97°C (30 s), 57°C (30 s), and 72°C (30 s); the products were then separated by agarose gel electrophoresis (12). Quantitative real-time PCR was carried out in a final volume of 25 μl containing the cDNA (amplified as described above), 2× PCR Master Mix (Applied Biosystems), and primers specific for 18S rRNA (Applied Biosystems) as an internal control or primers specific for *Aldh1a1*, *Aldh1a2*, or *Aldh1a3* (Applied Biosystems), using a 7700 Sequence Detector (Applied Biosystems). After incubation at 95°C for 10 min, products were amplified using 35 cycles of 95°C (15 s), 60°C (60 s), and 50°C (120 s).

### *Measurement of cytokines and IgA in culture supernatants*

The concentrations of IFN-γ, IL-17, IL-4, TNF-α, IL-6, IL-10, and IL-12p40 were measured using the Bio-plex system (Bio-Rad) following the manufacturer's instructions. The levels of IgA and IL-23 were determined by ELISA (R&D Systems and eBioscience, respectively).

### *In vitro IgA$^+$ plasma cell differentiation*

Peritoneal IgM$^+$IgD$^+$ cells ($1 \times 10^5$) were cultured in medium supplemented with BAFF (50 ng/ml) together with CD11c$^+$CD103$^+$CD8α$^+$ LPDCs ($2 \times 10^4$) in the presence or absence of poly I:C (50 μg/ml), R-848 (100 nM), CpG ODN (1 μM), or CD11c$^+$CD103$^+$CD8α$^-$ LPDCs ($2 \times 10^4$) in the presence or absence of flagellin (1 μg/ml) or CpG ODN (1 μM) for 5 d. After the depletion of DCs by anti-CD11c microbeads (Miltenyi Biotec), cells were analyzed by flow cytometry, and the concentration of IgA in the culture supernatants was determined by ELISA.

### *In vitro Treg differentiation*

OT-II Tg CD4$^+$ T cells ($1 \times 10^5$) were cultured in medium supplemented with TGF-β (1 ng/ml) and OVA protein (10 μg/ml) together with CD11c$^+$CD103$^+$CD8α$^+$ LPDCs ($2 \times 10^4$) in the presence or absence of poly I:C (50 μg/ml), R-848 (100 nM), CpG ODN (1 μM), or CD11c$^+$CD103$^+$CD8α$^-$ LPDCs ($2 \times 10^4$) in the presence or absence of flagellin (1 μg/ml) or CpG ODN (1 μM) for 4 d. After the depletion of DCs by anti-CD11c microbeads (Miltenyi Biotec), CD4$^+$ cells expressing Foxp3 were analyzed by flow cytometry.

### *In vitro helper CD4$^+$ T cell differentiation*

OT-II Tg CD4$^+$ T cells ($1 \times 10^5$) were cultured in medium supplemented with OVA protein (10 μg/ml) together with CD11c$^+$CD103$^+$CD8α$^+$ LPDCs ($2 \times 10^4$) in the presence or absence of poly I:C (50 μg/ml), R-848 (100 nM), CpG ODN (1 μM), or CD11c$^+$CD103$^+$CD8α$^-$ LPDCs ($2 \times 10^4$) in the presence or absence of flagellin (1 μg/ml) or CpG ODN (1 μM) for 4 d. The concentrations of IL-17, IFN-γ, and IL-4 in the culture supernatants were determined using the Bio-plex system (Bio-Rad). After the depletion of DCs by anti-CD11c microbeads (Miltenyi Biotec), CD4$^+$ cells expressing T-bet and RORγT were analyzed by flow cytometry. Cocultured cells were restimulated for 4 h with PMA (50 ng/ml; Sigma-Aldrich) and ionomycin (500 ng/ml; Calbiochem) in the presence of GolgiStop (BD Pharmingen) after the depletion of DCs by anti-CD11c microbeads. Then, CD4$^+$ cells producing IL-17 and IFN-γ were analyzed by flow cytometry.

### *In vitro CD8$^+$ T cell proliferation assay*

OT-I Tg CD8$^+$ T cells ($1 \times 10^5$) were cultured in triplicate with the indicated numbers of CD11c$^+$CD103$^+$CD8α$^+$ LPDCs in the presence or

absence of poly I:C (50 μg/ml), R-848 (100 nM), CpG ODN (1 μM), or $CD11c^+CD103^+CD8\alpha^-$ LPDCs ($2 \times 10^4$) in the presence or absence of flagellin (1 μg/ml) or CpG ODN (1 μM) in medium supplemented with OVA protein (10 μg/ml) for 96 h. Following this, 1 mCi [$^3$H]thymidine (Amersham Biosciences) was pulsed for the last 8 h, and then [$^3$H] uptake was measured in a scintillation counter (Packard Instruments).

### *Generation of OT-I CTL*

OT-I Tg $CD8^+$ T cells ($1 \times 10^6$) were cultured in medium supplemented with OVA protein (10 μg/ml) together with $CD11c^+CD103^+CD8\alpha^+$ LPDCs ($1 \times 10^5$) in the presence or absence of poly I:C (50 μg/ml), R-848 (100 nM), CpG ODN (1 μM), or $CD11c^+CD103^+CD8\alpha^-$ LPDCs ($1 \times 10^5$) in the presence or absence of flagellin (1 μg/ml) or CpG ODN (1 μM). On day 4 of culture, 10 U/ml recombinant human IL-2 (rhIL-2; R&D Systems) was added, and activated cells were further expanded in the presence of rhIL-2. On day 7 of culture, activated OT-I CTL were used as effectors in in vitro cytotoxicity assay.

### *In vitro cytotoxicity assay*

EL-4 cells were pulsed with or without 10 μg/ml $OVA_{257-264}$ peptide. After 60 min, targets were washed with 2% FCS/PBS to remove excess peptide and resuspended in PBS. Targets were labeled with 0.1 μM CFSE (Sigma-Aldrich) for 10 min at room temperature and washed twice. Targets were then plated out at $10^5$ cells/well in a 96-well U-bottom plate in a 100 μl volume. Media alone or $2 \times 10^6$ cells with effectors (activated OT-I CTL) were added and incubated for 5 h at 37°C/5% $CO_2$. After incubation, cells were stained with Kusabira-Orange–conjugated anti-Annexin V Ab for 20 min. Cells were then analyzed by flow cytometry. A gate was set on forward scatter versus CFSE to exclude effectors and measure cell death and apoptosis on targets. The percentage-specific lysis was calculated using the following formula: cytotoxicity (%) = $([ET - T_0]/[100 - T_0]) \times 100$, in which ET was the percentage of Annexin $V^+$ cells in $CFSE^+$ cells after the culture of targets and effectors, and $T_0$ was the percentage of Annexin $V^+$ cells in $CFSE^+$ cells after the culture of targets alone.

### *Immunization*

$CD11c^+CD103^+CD8\alpha^+$ LPDCs or $CD11c^+CD103^+CD8\alpha^-$ LPDCs were cultured for 12 h with OVA protein (100 μg/ml) in the presence of CpG ODN (1 μM). Ag-loading cells ($5 \times 10^4$ per mouse) were injected on days 0 and 14 into the peritoneal cavities of naive $Tlr9^{-/-}$ mice; control mice were treated with PBS.

### *Detection of Ag-specific Ab titers*

One week after the final immunization, serum and fecal extracts were obtained from the immunized and control mice. For determination of OVA-specific IgG titers in the sera or IgA titers in the fecal extracts, 96-well microtiter plates (Corning) were coated overnight at 4°C with 200 μg/ml OVA in 50 mM carbonate buffer (pH 9.6). Plates were blocked with PBS containing 1% fraction V BSA (Serologicals Proteins) at 37°C for 1 h. Test sera were serially diluted with PBS containing 0.2% BSA and 0.02% Tween 20 and incubated at 37°C for 2 h. After incubation, HRP-conjugated goat anti-mouse IgG or IgA (Zymed), diluted 1:2000 in PBS containing 0.2% BSA and 0.02% Tween 20, was added and incubated at 37°C for 1 h. Wells were washed five times with PBS containing 0.02% Tween 20 between each step. Plates were developed at room temperature following the addition of *o*-phenylendiamine (0.4 mg/ml) and hydrogen peroxide (0.012%) in 7 mM citrate buffer (pH 5). Finally, 1 M $H_2SO_4$ was added, and absorbance was measured at 490 nm with a microplate reader (model 550; Bio-Rad). Preimmunized serum was used as a negative control. The average extinction in negative control wells, to which three times the SD was added, provided the reference point for determination of the titer in the test sera. Ab titers were expressed as the reciprocal of the last dilution yielding an extinction value higher than the reference value.

### *Ag-specific cytokine production in T cells*

One week after the final immunization, splenocytes were collected from the immunized and control mice and were cultured for 4 d with the $OVA_{257-264}$ peptide (10 μg/ml) or $OVA_{323-339}$ peptide (10 μg/ml). The concentration of IFN-γ ($OVA_{257-264}$ and $OVA_{323-339}$), IL-17 ($OVA_{323-339}$), and IL-4 ($OVA_{323-339}$) in the culture supernatants was measured using the Bio-plex system (Bio-Rad).

### *In vivo cytotoxicity assay*

C57BL/6 splenocytes were labeled with either 0.5 or 5 μM CFSE for 15 min at room temperature and washed twice. $CFSE^{bright}$ cells (M2) were subsequently pulsed with 0.5 μg/ml $OVA_{257-264}$ for 90 min at 37°C. The $CFSE^{dull}$ cells (M1) remained unpulsed. Cells were mixed at a 1:1 ratio, and then a total of $5 \times 10^6$ cells was injected i.v. into the immunized or control mice.

### *Statistical analysis*

Statistical significance was evaluated using an unpaired two-tailed Student *t* test in all experiments. A $p$ value $<0.05$ was considered significant.

## Results

### *$CD103^+$ LPDCs were divided into two subsets*

DCs comprise a heterogenous population of APCs, which include plasmacytoid DCs and $CD11c^{hi}$ conventional DCs (cDCs) (15). Mouse cDCs in lymphoid tissues include $CD8\alpha^+$ and $CD8\alpha^-$ subsets that have distinct functional properties. $CD103^+$ DCs are a major cDC subset in the intestinal LP (7). Similar to cDCs in lymphoid tissues, we found that $CD11c^+CD103^+$ cells in the small intestinal LP were divided into $CD8\alpha^+$ and $CD8\alpha^-$ subsets (Fig. 1*A*). Our previous report showed that $CD11c^+$ LPCs in the small intestine consisted of four subsets: $CD11c^{hi}CD11b^{lo}$ DCs, $CD11c^{hi}CD11b^{hi}$ DCs, $CD11c^{int}CD11b^{int}$ macrophages, and $CD11c^{int}CD11b^{mid}$ eosinophils (12). Flow cytometry analysis indicated that $CD11c^+CD103^+CD8\alpha^+$ cells converged on the $CD11c^{hi}CD11b^{lo}$ subset, whereas $CD11c^+CD103^+CD8\alpha^-$ cells were predominantly in the $CD11c^{hi}CD11b^{hi}$ subset (Fig. 1*A*). Although both $CD11c^{hi}CD11b^{lo}$ and $CD11c^{hi}CD11b^{hi}$ DC subsets are $CD103^+$ in the intestinal LP (Fig. 1*B*) (12), only $CD11c^{hi}$ $CD11b^{lo}$ LPDCs expressed CD8α (Fig. 1*C*). These findings suggest that $CD103^+$ LPDCs are divided into $CD8\alpha^+$ and $CD8\alpha^-$ subsets, which were equivalent to $CD11c^{hi}CD11b^{lo}$ and $CD11c^{hi}$ $CD11b^{hi}$ LPDCs, respectively.

### *$CD103^+CD8\alpha^+$ LPDCs express TLR3, TLR7, and TLR9*

We previously showed that $CD11c^{hi}CD11b^{hi}$ LPDCs specifically express TLR5 and have unique properties to mediate innate and acquired immune responses induced by flagellin stimulation (12). To examine the immunological function of the newly identified $CD103^+CD8\alpha^+$ LPDC subset, we isolated $CD11c^{hi}CD103^+CD8\alpha^+$ cells by FACS sorting. $CD11c^{hi}CD103^+CD8\alpha^-$ cells ($CD103^+$ $CD8\alpha^-$ LPDCs) were used as controls for the following experiments. We first checked the expression patterns of TLR family members. Whereas $CD103^+CD8\alpha^-$ LPDCs expressed TLR5 and TLR9, $CD103^+CD8\alpha^+$ LPDCs expressed TLR3, TLR7, and TLR9

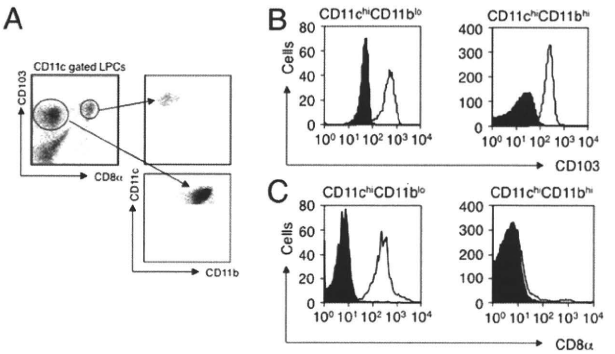


**FIGURE 1.** $CD103^+$ LPDCs are divided into two populations. *A*, Small intestinal LPDCs were stained for CD11b, CD11c, CD103, and CD8α. Live $CD11c^+$ cells were analyzed for the expression of CD103 and CD8α (*left panel*). $CD11c^+CD103^+CD8\alpha^+$ and $CD11c^+CD103^+CD8\alpha^-$ cells were further analyzed for the expression of CD11b (*right panel*). *B*, Surface expression of CD103 on $CD11c^{hi}CD11b^{lo}$ or $CD11c^{hi}CD11b^{hi}$ LPDCs. *C*, Surface expression of CD8α on $CD11c^{hi}CD11b^{lo}$ or $CD11c^{hi}CD11b^{hi}$ LPCs. ■, isotype control; □, stained cells.

(Fig. 2*A*). As shown in our previous study, the CD11c$^{hi}$CD11b$^{hi}$ subset, which correspond to CD103$^+$CD8α$^-$ LPDCs, produced IL-6 and IL-12 p40 in response to flagellin and CpG ODN (12). We stimulated CD103$^+$CD8α$^+$ and CD103$^+$CD8α$^-$ LPDCs with their respective TLR ligands and checked proinflammatory cytokine production (Fig. 2*B*). Consistent with the previous results, CD103$^+$CD8α$^-$ LPDCs produced IL-6 and IL-12 p40 in response to flagellin and CpG ODN. Similarly, CD103$^+$CD8α$^+$ LPDCs produced IL-6 and IL-12p40 in response to their respective ligands, poly I:C, R-848, and CpG ODN. However, TNF-α, IL-23, or IL-10 were not induced in either cell subset.

### *CD103$^+$CD8α$^+$ LPDCs are not involved in T cell-independent IgA synthesis*

We next investigated the role of CD103$^+$CD8α$^+$ LPDCs in the activation of adaptive immune responses. We previously showed that the CD11c$^{hi}$CD11b$^{hi}$ subset in the LP specifically expresses *Raldh2* and is involved in T cell-independent IgA class-switch recombination of B cells (12, 13). We examined the involvement of CD103$^+$CD8α$^+$ LPDCs in IgA synthesis. We first checked whether CD103$^+$CD8α$^+$ LPDCs synthesize RA and found that whereas CD103$^+$CD8α$^-$ LPDCs specifically expressed *Raldh2*, no expression of RALDH isoforms was detected in CD103$^+$CD8α$^+$ LPDCs (Fig. 3*A*). Thus, RA-producing CD103$^+$ DCs in the LP belong to the CD8α$^-$ subset (CD11c$^{hi}$CD11b$^{hi}$) and not the CD8α$^+$ subset (CD11c$^{hi}$CD11b$^{lo}$). We further examined whether CD103$^+$CD8α$^+$ LPDCs could induce T cell-independent IgA class switching, demonstrating that although flagellin- and CpG ODN-stimulated CD103$^+$CD8α$^-$ LPDCs efficiently induced the differentiation of B220$^-$IgA$^+$ plasma cells, stimulation of CD103$^+$CD8α$^+$ LPDCs via TLR3, TLR7, or TLR9 did not (Fig. 3*B*). Consistent with the FACS data, IgA production was not detected in the supernatants of naive B cells cocultured with CD103$^+$CD8α$^+$ LPDCs and stimulated with TLR ligands (Fig. 3*C*). Taken together, these findings suggest that CD103$^+$CD8α$^+$ LPDCs are not able to induce T cell-independent differentiation of IgA$^+$ plasma cells.

### *CD103$^+$CD8α$^+$ LPDCs do not induce Foxp3$^+$ Tregs*

Previous reports have shown that CD103$^+$ DCs isolated from the LP or from the MLNs promote the differentiation of Foxp3$^+$ Tregs, an activity dependent on RA and TGF-β (8, 10). We examined whether CD103$^+$CD8α$^+$ and CD103$^+$CD8α$^-$ LPDCs could induce Treg conversion. Naive OVA-specific OT-II Tg CD4$^+$ T cells were cocultured with CD103$^+$CD8α$^+$ or CD103$^+$CD8α$^-$ LPDCs together with or without the indicated TLR ligand in the presence of OVA protein and TGF-β (Fig. 4). CD103$^+$CD8α$^-$ LPDCs could not induce the conversion of Foxp3$^+$ Tregs regardless of TLR ligand stimulation. In contrast, CD103$^+$CD8α$^-$ LPDCs, which express Raldh2, promoted the differentiation of Foxp3$^+$ Tregs. Furthermore, stimulation with both flagellin and CpG ODN reduced Foxp3$^+$ Treg induction. However, even CD103$^+$CD8α$^-$ LPDCs could not induce Foxp3$^+$ Tregs in the absence of TGF-β (data not shown). Thus, CD103$^+$CD8α$^-$ but not CD103$^+$CD8α$^+$ LPDCs effectively induced Foxp3$^+$ Tregs in the presence of TGF-β in the absence of TLR activation.

### *CD4$^+$ Th cell responses in CD103$^+$CD8α$^+$ LPDCs*

We next assessed the ability of CD103$^+$CD8α$^+$ LPDCs to induce Ag-specific Th cell differentiation in OVA-specific OT-II Tg CD4$^+$ T cells. As shown in our previous study, CD11c$^{hi}$CD11b$^{hi}$ LPDCs induced Th1 and Th17 cells in response to flagellin and CpG ODN (12). We could detect both IFN-γ– and IL-17–producing cells in cocultures of OT-II CD4$^+$ T cells and CD103$^+$CD8α$^-$ LPDCs stimulated by flagellin and CpG ODN (Fig. 5*A*). However, only IFN-γ–producing cells were detected in cocultures of OT-II CD4$^+$ T cells and CD103$^+$CD8α$^+$ LPDCs stimulated by poly I:C, R-848, and CpG ODN. Both CD103$^+$CD8α$^+$ LPDCs stimulated by poly I:C, R-848, and CpG ODN and CD103$^+$CD8α$^-$ LPDCs stimulated by flagellin and CpG ODN induced high expression of T-bet, a lineage-determining factor for Th1 cells in naive CD4$^+$ T cells (Supplemental Fig. 1*A*). Furthermore, expression of RORγT, the key transcription factor in Th17 cells was upregulated in naive CD4$^+$ T cells together with CD103$^+$CD8α$^-$ LPDCs stimulated by flagellin and CpG ODN (Supplemental Fig. 1*B*). Consistent with the flow

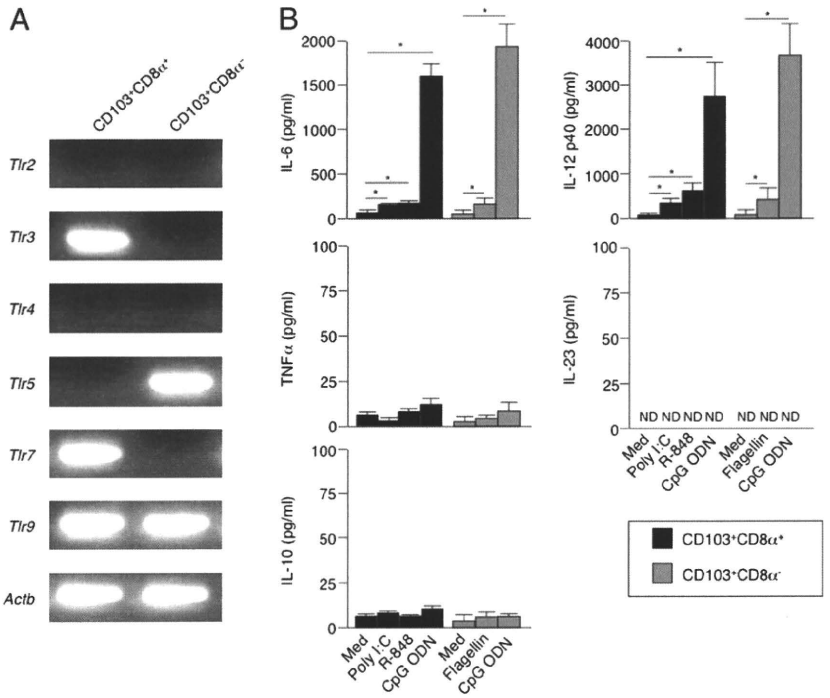


**FIGURE 2.** TLR expression in CD103$^+$ CD8α$^+$ LPDCs. *A*, Expression of mRNA encoding the indicated genes in CD103$^+$CD8α$^+$ and CD103$^+$CD8α$^-$ LPDCs. Data are representative of three independent experiments. *B*, Cytokine production by CD103$^+$CD8α$^+$ and CD103$^+$CD8α$^-$ LPDCs in response to medium alone (Med) or indicated TLR ligands. Data represent the means ± SD from three independent experiments. $^*p < 0.05$. ND, not detected.

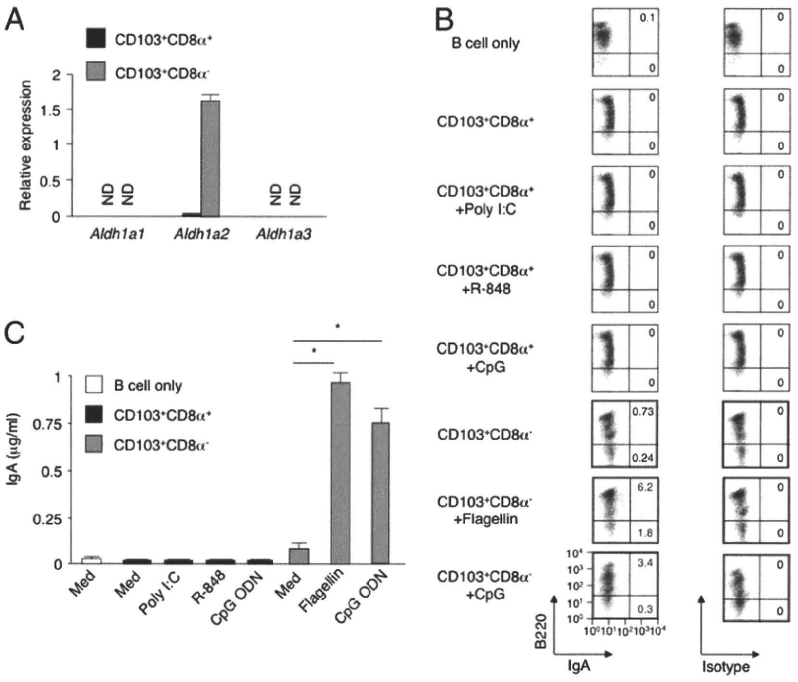


**FIGURE 3.** CD103$^+$CD8α$^+$ LPDCs are not involved in T cell-independent IgA synthesis. *A*, Quantitative PCR of mRNA encoding RALDH isozymes in CD103$^+$CD8α$^+$ and CD103$^+$CD8α$^-$ LPDCs. Data are representative of three independent experiments. *B* and *C*, Peritoneal IgM$^+$ IgD$^+$ cells were cultured in the indicated conditions for 5 d. *B*, Cells were stained for B220 and IgA. Numbers in quadrants indicate percentage of B220$^+$ IgA$^+$ cells (*top right panel*) or B220$^-$IgA$^+$ cells (*bottom right panel*). Data are representative of three independent experiments. *C*, Concentration of IgA in the coculture supernatants. Data represent the means ± SD from three independent experiments. *$p < 0.05$. ND, not detected.

cytometry analysis, both IFN-γ and IL-17 were significantly induced in cocultures with CD103$^+$CD8α$^-$ LPDCs stimulated by flagellin and CpG ODN (Fig. 5*B*). In contrast, only IFN-γ was significantly induced in cocultures with CD103$^+$CD8α$^+$ LPDCs stimulated by poly I:C, R-848, and CpG ODN. Taken together, these findings suggest that activated CD103$^+$CD8α$^+$ LPDCs induced phenotypic and functional Th1 cells but not Th17 cells in vitro.

### *In vitro CD8$^+$ T cell proliferation by CD103$^+$CD8α$^+$LPDCs*

Soluble and cell-associated Ags can be presented to CD8$^+$ T cells in an MHC class I-restricted manner (16), a process referred to as cross-presentation. It is believed that CD8α$^+$ DCs but not CD8α$^-$ DCs are responsible for cross-presentation in the spleen (17). To examine whether CD103$^+$CD8α$^+$ LPDCs contribute to the presentation of Ag to CD8$^+$ T cells in vitro, we checked their ability to stimulate the proliferation of OVA-specific CD8$^+$ T cells from OT-I Tg mice (Fig. 6*A*). Although the proliferation of CD8$^+$ T cells was low when they were cocultured with CD103$^+$CD8α$^+$ LPDCs, treatment of the DCs with poly I:C, R-848, and CpG ODN strongly stimulated CD8$^+$ T cell proliferation. Similarly, flagellin- and CpG ODN-stimulated CD103$^+$CD8α$^-$ LPDCs potently induced the proliferation of CD8$^+$ T cells. Thus, both CD103$^+$CD8α$^+$ and CD103$^+$CD8α$^-$ LPDCs activated by TLR ligands were capable of stimulating proliferation of CD8$^+$ T cells in vitro. We next examined the cytotoxic activity of OT-I CTL induced by CD103$^+$CD8α$^+$ LPDCs and CD103$^+$CD8α$^-$ LPDCs in vitro. OT-I CTL induced by CD103$^+$CD8α$^+$ LPDCs specifically killed the $OVA_{257–264}$ peptide-pulsed target cells (Fig. 6*B*). Treatment of the CD103$^+$CD8α$^+$ LPDCs with poly I:C, R-848, and CpG ODN further increased cytotoxicity of OT-I CTL. Similarly, OT-I CTL induced by CD103$^+$CD8α$^-$ LPDCs specifically killed the targets pulsed with $OVA_{257–264}$ peptide. Flagellin and CpG ODN treatment enhanced cytotoxic activity in CD8$^+$ T cells. Taken together, both CD103$^+$CD8α$^+$ and CD103$^+$CD8α$^-$ LPDCs activated by TLR ligands strongly induced CTL in vitro.

### *In vivo immune responses by CD103$^+$CD8α$^+$ LPDCs*

We finally compared the adaptive immune responses in mice immunized with Ag-loaded CD103$^+$CD8α$^+$ LPDCs. We isolated CD103$^+$CD8α$^+$ and CD103$^+$CD8α$^-$ LPDCs from C57BL/6 mice

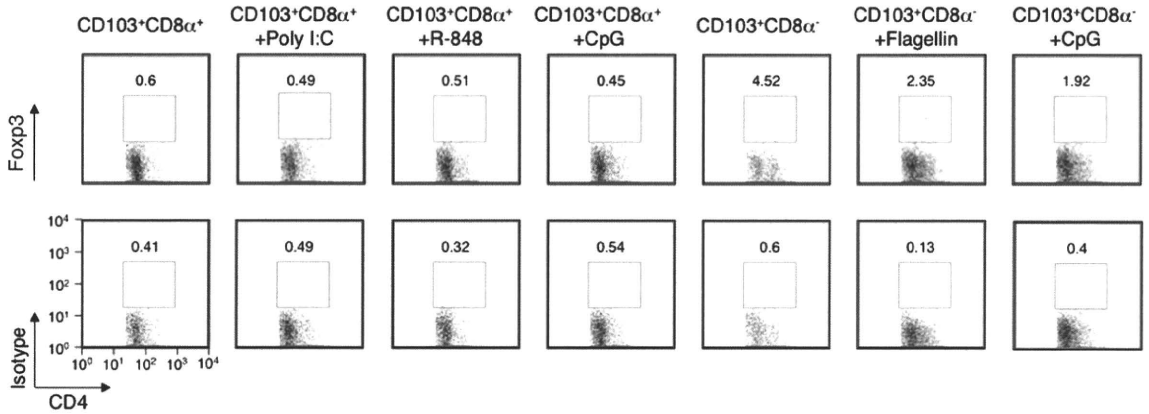


**FIGURE 4.** CD103$^+$CD8α$^+$ LPDCs do not induce Foxp3$^+$ Tregs. Flow cytometry of OT-II Tg CD4$^+$ T cells cultured in the presence of TGF-β (1 ng/ml) for 4 d at the indicated conditions and stained intracellularly for Foxp3 and isotype controls. Numbers in the gated areas indicate percentage of CD4$^+$Foxp3$^+$ cells. Data are representative of three independent experiments.

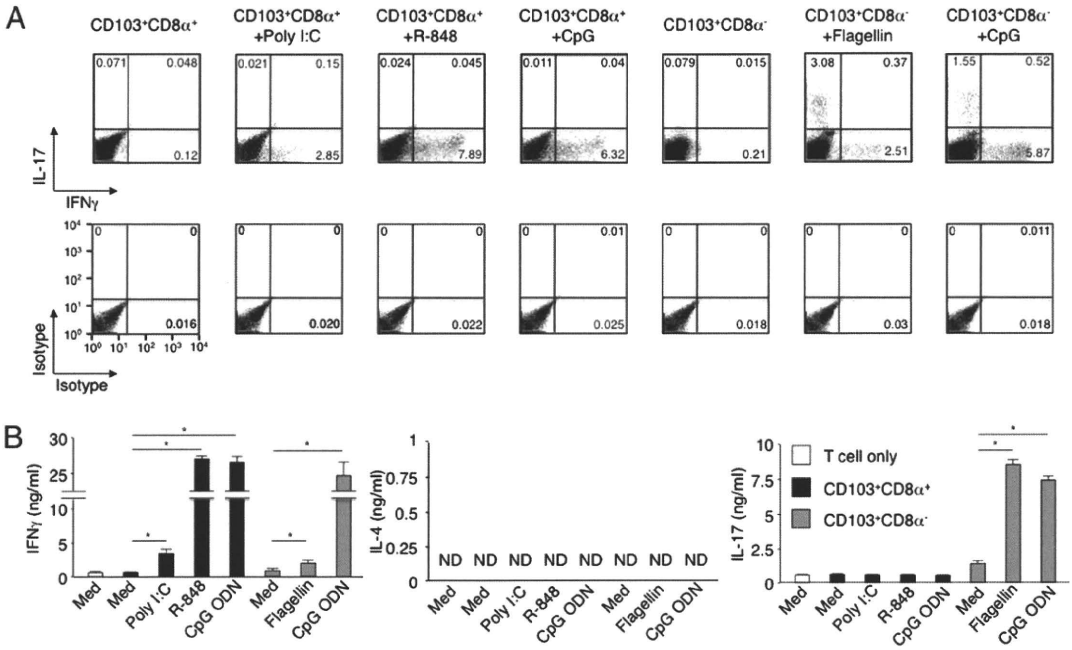


**FIGURE 5.** CD4$^+$ T cell stimulation by CD103$^+$CD8α$^+$ LPDCs. *A*, Flow cytometry of OT-II Tg CD4$^+$ T cells cultured for 4 d under the indicated conditions and stained intracellularly for IL-17, IFN-γ (*top panels*), and isotype controls (*bottom panels*). Numbers in quadrants indicate percentage of IL-17$^+$IFN-γ$^-$ cells (*top left panel*), IL-17$^+$IFN-γ$^+$ cells (*top right panel*), or IL-17$^-$IFN-γ$^+$ cells (*bottom right panel*). Data are representative of three independent experiments. *B*, OT-II Tg CD4$^+$ T cells were cultured in the indicated conditions for 4 d. IFN-γ, IL-4, and IL-17 production in the coculture supernatants. Data represent the means ± SD from three independent experiments. $*p < 0.05$. ND, not detected.

and cultured them with OVA protein (100 μg/ml) overnight. For optimum activation of Ag-loaded DCs, we added CpG DNA (1 μM), a mutual TLR ligand for CD103$^+$CD8α$^+$ and CD103$^+$CD8α$^-$ LPDCs, to the culture media. Ag-loaded cells ($1 \times 10^5$) were injected into the peritoneal cavities of *Tlr9*$^{-/-}$ mice on days 0 and 14, whereas control mice were treated with PBS. One week after the second injection, the DC vaccination-induced Ag-specific B cell responses were analyzed. Groups of mice immunized with both CD103$^+$CD8α$^+$ and CD103$^+$CD8α$^-$ LPDCs showed significantly higher levels of serum OVA-specific IgG Ab (Fig. 7*A*). In addition, high titers of OVA-specific IgA were detected in fecal extracts from CD103$^+$CD8α$^-$ LPDC-immunized mice. These results indicated that CD103$^+$CD8α$^+$ LPDCs induced Ag-specific IgG in sera, whereas CD103$^+$CD8α$^-$ LPDCs induced Ag-specific IgG in sera as well as Ag-specific IgA in the intestinal compartments.

We next examined the Th cell responses of mice immunized with Ag-loaded LPDCs. One week after the second injection, spleen cells from the immunized mice were cultured in the presence of OVA class II peptide ($OVA_{323-339}$). As shown in our previous study, we detected OVA class II peptide-specific IFN-γ production as well as IL-17 production after injection of CD103$^+$CD8α$^-$

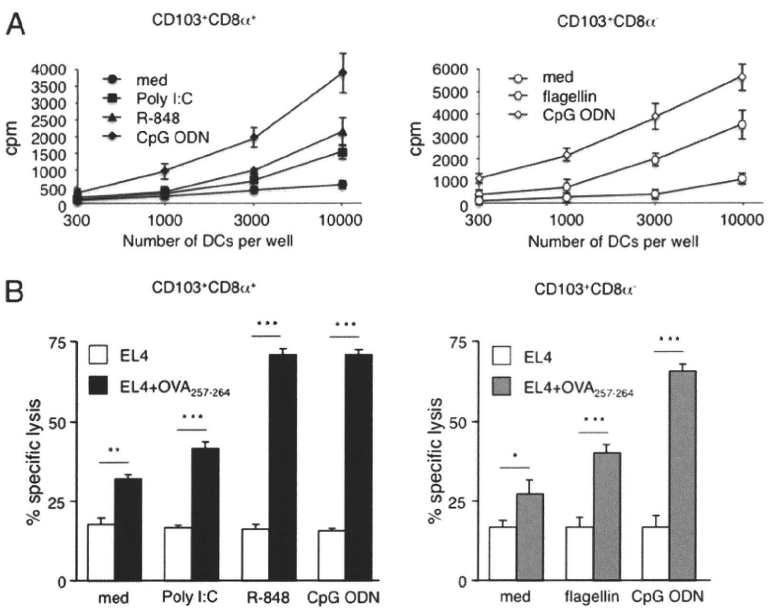


**FIGURE 6.** CD8$^+$ T cell stimulation by CD103$^+$ CD8α$^+$ LPDCs. *A*, OT-I Tg CD8$^+$ T cells were cultured in the indicated conditions for 4 d. Total of 1 mCi [$^3$H]thymidine was pulsed for the last 8 h, and [$^3$H] incorporation was measured using a β scintillation counter. Results are the average of triplicate wells ± SEM. Data are representative of three independent experiments. *B*, OT-I Tg CD8$^+$ T cells were cultured in the indicated conditions for 4 d. Activated CD8$^+$ T cells were further expanded in the presence of rhIL-2 for following 3 d. OT-I CTLs were tested for cytotoxicity against EL4 pulsed with or without $OVA_{257-264}$ peptide at an E:T ratio of 20:1 for 5 h. Data represent the means ± SD from three independent experiments. $*p < 0.05$, $**p < 0.01$, $***p < 0.005$.

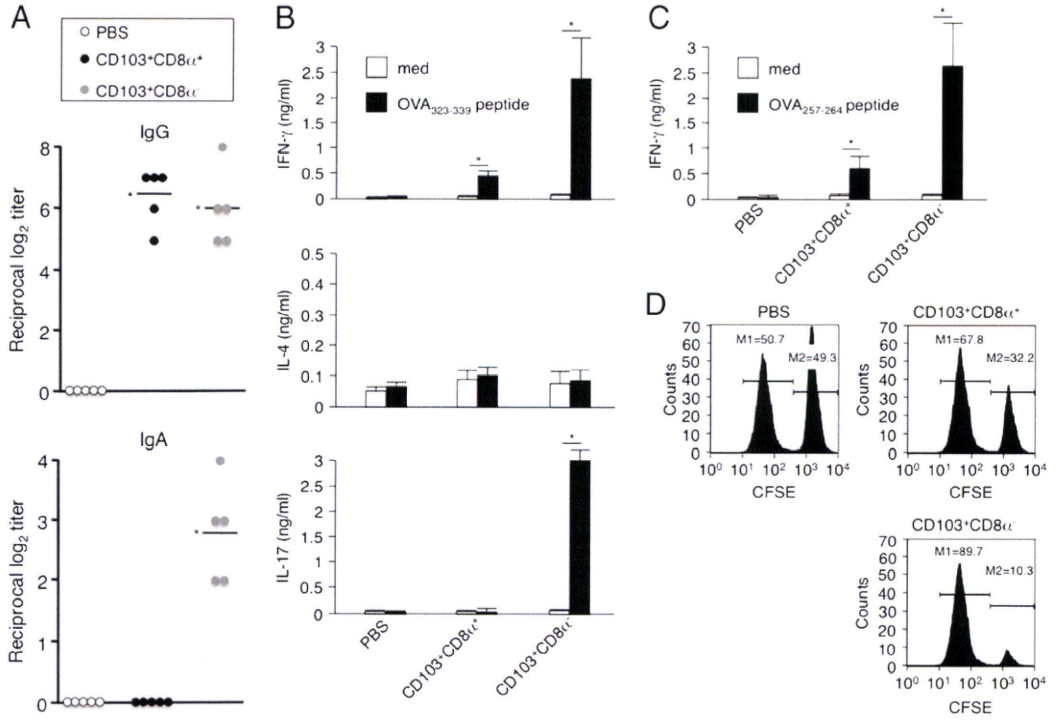


**FIGURE 7.** In vivo immune responses by $CD103^+CD8\alpha^+$ LPDCs. *A–D*, $CD103^+CD8\alpha^+$ or $CD103^+CD8\alpha^-$ LPDCs cultured for 12 h with OVA protein (100 μg/ml) in the presence of CpG ODN (1 μM) were injected on days 0 and 14 into the peritoneal cavities of naive *Tlr9*$^{-/-}$ mice at a dose of $5 \times 10^4$ Ag-loaded cells per mouse; control mice were treated with PBS. *A*, One week after the final immunization, titers of Ag-specific serum total IgG and fecal extract IgA were measured by ELISA. Open circle, PBS ($n = 5$); black circle, $CD103^+CD8\alpha^+$ ($n = 5$); gray circle, $CD103^+CD8\alpha^-$ ($n = 5$). $^*p < 0.05$ versus PBS. One week after the final immunization, splenocytes ($n = 5$ per each group) were collected and cultured for 4 d with 10 μg/ml $OVA_{323-339}$ peptide (*B*) or $OVA_{257-264}$ peptide (*C*) before measurement of IFN-γ (*B*, *C*), IL-17 (*B*), and IL-4 (*B*) in culture supernatants. Data represent the means ± SD from two independent experiments. *D*, In vivo cytotoxic activity induction in mice immunized with PBS, $CD103^+CD8\alpha^+$, or $CD103^+CD8\alpha^-$ LPDCs. Target cells were prepared as described in the *Materials and Methods*. OVA-specific cytolytic activity was measured in vivo following i.v. injection of equal numbers of $CFSE^{bright}$ cells pulsed with $OVA_{257-264}$ peptide and nonpulsed $CFSE^{dull}$ splenocytes used as targets into immunized mice at day 21. In vivo cytolysis of these target cells was assed ex vivo by flow cytometry analysis of $CFSE^{dull}$ or $CFSE^{bright}$ cells in the spleen. Numbers above peaks represent the relative percentage of $CFSE^{dull}$ (M1) or $CFSE^{bright}$ (M2) cells. Data are representative of three independent experiments. $^*p < 0.05$. ND, not detected.

LPDCs (Fig. 7*B*) (12). In contrast, only IFN-γ was produced by splenocytes from mice injected with $CD103^+CD8\alpha^-$ LPDCs. These results suggested that $CD103^+CD8\alpha^+$ LPDCs induced Th1 response but not Th17 response in vivo.

To further examine the Ag-specific $CD8^+$ T cell response, spleen cells from immunized mice were cultured in the presence of OVA class I peptide ($OVA_{257-264}$), and IFN-γ levels were measured. We detected OVA class I peptide-specific IFN-γ production after injection of both $CD103^+CD8\alpha^+$ and $CD103^+CD8\alpha^-$ LPDCs (Fig. 7*C*). However, the class I-restricted IFN-γ level was much lower after $CD103^+CD8\alpha^+$ LPDC immunization than after $CD103^+CD8\alpha^-$ LPDC immunization, despite the injection of the same numbers of Ag-loaded DCs stimulated with the same TLR ligand, CpG ODN. We then evaluated the cytotoxic activity of the Ag-specific $CD8^+$ T cells after $CD103^+CD8\alpha^+$ and $CD103^+CD8\alpha^-$ LPDC immunization. To detect potential OVA-specific cytotoxicity of CTLs in immunized mice, we used an in vivo cytotoxicity assay consisting of an i.v. infusion of $OVA_{257-264}$ peptide-pulsed $CFSE^{bright}$ target cells and nonpulsed $CFSE^{dull}$ target cells followed by subsequent ex vivo quantification of the remaining $OVA_{257-264}$ peptide-pulsed $CFSE^{bright}$ target cells in spleen cell suspensions by flow cytometry. Partial lysis of $CFSE^{bright}$ target cells was observed in the mice immunized with $CD103^+CD8\alpha^+$ LPDCs, whereas $CFSE^{bright}$ target cells were effectively lysed in mice immunized with $CD103^+CD8\alpha^-$ LPDCs (Fig. 7*D*), correlating with the $OVA_{257-264}$ peptide-specific IFN-γ production findings.

## Discussion

$CD103^+$ DCs are the major population of APCs present in the intestinal LP. They have been thought of as a monosubset of DCs and were originally identified through their induction of $Foxp3^+$ Tregs via their derived RA (8, 10). Therefore, $CD103^+$ LPDCs have been considered to be regulators of intestinal immunity, which induce tolerance and maintain intestinal homeostasis. In this study, we found that $CD103^+$ LPDCs in the small intestine are divided into distinct subsets: a small $CD8\alpha^+$ subset and a large $CD8\alpha^-$ subset. Our previous study showed that there existed two subsets of DCs in intestinal LP: $CD11c^{hi}CD11b^{low}$ and $CD11c^{hi}CD11b^{hi}$ (12). The $CD11c^{hi}CD11b^{low}$ and $CD11c^{hi}CD11b^{hi}$ subsets had a DEC-205$^+$, MHC class II high, $CD80^+CD86^+$ surface phenotype. In addition, the $CD11c^{hi}CD11b^{hi}$ subset is moderately F4/80 positive, suggesting that this subset expresses both DC (DEC-205) and macrophage (F4/80) markers (12). According to the flow cytometry analysis, $CD103^+CD8\alpha^+$ and $CD103^+CD8\alpha^-$ LPDCs were equivalent to $CD11c^{hi}CD11b^{lo}$ and $CD11c^{hi}CD11b^{hi}$ subsets, respectively (Fig. 1*A*).

In this study, we analyzed the immunological function of the newly identified $CD8\alpha^+$ conventional DCs in the small intestinal LP for the first time, to our knowledge. $CD103^+CD8\alpha^+$ LPDCs showed different TLR family member expression profiles from $CD103^+CD8\alpha^-$ LPDCs. Whereas $CD103^+CD8\alpha^-$ LPDCs expressed TLR5 and TLR9, $CD103^+CD8\alpha^+$ LPDCs expressed TLR3, TLR7, and TLR9, which recognize dsRNA, ssRNA, and CpG ODN, respectively (Fig. 2*A*). However, both LPDC types

produced proinflammatory cytokines, such as IL-6 and IL-12p40, but not the anti-inflammatory cytokine IL-10, in response to their respective TLR ligands, suggesting that CD103$^+$CD8$\alpha^+$ and CD103$^+$CD8$\alpha^-$ LPDCs induce inflammatory responses after TLR ligand stimulation (Fig. 2*B*).

Both DC subsets were CD103$^+$; however, only CD8$\alpha^-$ LPDCs expressed the mRNA of RA-converting enzyme Raldh2 (Fig. 3*A*). Consistent with *Raldh2* expression, CD103$^+$CD8$\alpha^-$ LPDCs induced Foxp3$^+$ Tregs in the presence of TGF-β (Fig. 4). These data suggested that CD8$\alpha^-$ LPDCs but not CD8$\alpha^+$ LPDCs are responsible for the regulatory functions of CD103$^+$ DCs in the LP. Accordingly, CD103$^+$CD8$\alpha^+$ LPDCs may not have the ability to induce immunological tolerance in the small intestinal LP.

Although Ag-specific IgG induction is essential for the resolution of systemic infection, secretory IgA is critical for the protection of mucosal surfaces against viruses, bacteria, and toxins by direct neutralization or prevention of binding to the mucosal surface (18). Ag-specific IgA induction is important in preventing bacterial and viral infection. RA has been shown to have a direct IgA-promoting effect on B cells (12, 19). Both Ag-loaded CD103$^+$CD8$\alpha^+$ and CD103$^+$CD8$\alpha^-$ LPDCs induced high titers of Ag-specific IgG in serum. However, in accordance with *Raldh2* expression, only CD103$^+$CD8$\alpha^-$ LPDCs could induce T cell-independent IgA synthesis in vitro and Ag-specific IgA in stool samples (Figs. 3*B*, 3*C*, 7*A*). Thus, CD103$^+$CD8$\alpha^+$ LPDCs are not involved in IgA synthesis in the small intestinal LP.

T cell-dependent immune responses are polarized by the activation of different CD4$^+$ T cells, which produce individual patterns of cytokines. Both CD103$^+$CD8$\alpha^+$ and CD103$^+$CD8$\alpha^-$ LPDCs induced Ag-specific Th1 cells following TLR ligand stimulation (Figs. 5*A*, 5*B*, 7*B*). In addition to Th1 cells, CD103$^+$CD8$\alpha^-$ LPDCs induced Ag-specific Th17 cells. Thl cells secrete IL-2 and IFN-γ and predominate in cellular immune responses, particularly during intracellular infections. Th17 cells were reported to have important roles in a variety of inflammatory diseases, though it still remains unclear whether Th17 cells contribute to host protection and inflammation (20). Th17 cytokines such as IL-17A, IL-17F, and IL-22 have been shown to be critical for eliminating extracellular pathogens, suggesting that Th17 cells may play crucial roles in host defense against extracellular pathogens (21–24). Therefore, CD103$^+$CD8$\alpha^-$ LPDC-mediated immunization may be more effective than CD103$^+$CD8$\alpha^+$ LPDC-mediated immunization in the prevention of infectious diseases due to the induction of both Th1 and Th17 cells.

We finally examined the Ag-specific CD8$^+$ T cell response mediated by CD103$^+$CD8$\alpha^+$ and CD103$^+$CD8$\alpha^-$ LPDCs. CD103$^+$CD8$\alpha^+$ LPDCs and CD103$^+$CD8$\alpha^-$ LPDCs induced the proliferation and cytotoxicity of CD8$^+$ T cells in response to TLR ligand stimulation in vitro (Fig. 6). Although we injected the same numbers of Ag-loaded DCs stimulated with CpG ODN, class I-restricted IFN-γ levels and cytotoxic activity after CD103$^+$CD8$\alpha^-$ LPDC immunization were much higher than those after CD103$^+$CD8$\alpha^+$ LPDC immunization (Fig. 7*C*, 7*D*). Haan et al. (17) demonstrated that cell-associated Ag is cross-presented by CD8$\alpha^+$ DCs but not CD8$\alpha^-$ DCs in the spleen. Furthermore, i.v.-injected soluble Ags were cross-presented by CD8$\alpha^+$ DCs in the spleen. In contrast, CD8$\alpha^-$CD11b$^+$ DCs were generally involved in CD4$^+$ T cell responses to soluble Ags (25). Therefore, CD8$\alpha^+$ DCs in the spleen are believed to be responsible for cross-presentation to CD8$^+$ T cells. However, CD103$^+$CD8$\alpha^-$ LPDCs induced Ag-specific CTLs more effectively than CD103$^+$CD8$\alpha^+$ LPDCs. Furthermore, both TLR activated CD103$^+$CD8$\alpha^+$ and CD103$^+$CD8$\alpha^-$ LPDCs effectively induced CD4$^+$ Th responses. A previous study showed that CD8$\alpha^+$ and CD8$\alpha^-$CD11b$^{lo}$ DCs in Peyer's patches take up viral Ags from reovirus-infected intestinal epithelial cells and can present them to CD4$^+$ T cells (26). In addition, CD8$\alpha^-$CD11b$^-$ DCs as well as CD8$\alpha^+$ DCs present viral Ags to CD8$^+$ T cells during viral infection in the airway (27). Moreover, Chung et al. (28) demonstrated that CD8$\alpha^-$CD11b$^+$ DCs rather than CD8$\alpha^+$ DCs cross-present intestinal Ags to CD8$^+$ T cells in MLNs. Hence, within the mucosal-associated lymphoid tissues, cross-presentation may be mediated by CD8$\alpha^-$ DCs.

In summary, our data suggest that CD103$^+$CD8$\alpha^+$ and CD103$^+$CD8$\alpha^-$ LPDCs have divergent functions in active immunity. Based on the results obtained in this study, from both quantitative and qualitative viewpoints, CD103$^+$CD8$\alpha^+$ LPDCs may be less suitable targets for oral vaccines than CD103$^+$CD8$\alpha^-$ LPDCs in the small intestine. Further analysis of these two CD103$^+$ DC subsets as well as their functional cross talk is needed for a better understanding of how the intestinal immunity is regulated to finely tune the innate and adaptive systems.

## Acknowledgments

We thank N. Kitagaki for technical assistance and E. Kamada for secretarial assistance.

## Disclosures

The authors have no financial conflicts of interest.

## References

1. Iwasaki, A. 2007. Mucosal dendritic cells. *Annu. Rev. Immunol.* 25: 381–418.
2. Bogunovic, M., F. Ginhoux, J. Helft, L. Shang, D. Hashimoto, M. Greter, K. Liu, C. Jakubzick, M. A. Ingersoll, M. Leboeuf, et al. 2009. Origin of the lamina propria dendritic cell network. *Immunity* 31: 513–525.
3. Varol, C., A. Vallon-Eberhard, E. Elinav, T. Aychek, Y. Shapira, H. Luche, H. J. Fehling, W. D. Hardt, G. Shakhar, and S. Jung. 2009. Intestinal lamina propria dendritic cell subsets have different origin and functions. *Immunity* 31: 502–512.
4. Rescigno, M., M. Urbano, B. Valzasina, M. Francolini, G. Rotta, R. Bonasio, F. Granucci, J. P. Kraehenbuhl, and P. Ricciardi-Castagnoli. 2001. Dendritic cells express tight junction proteins and penetrate gut epithelial monolayers to sample bacteria. *Nat. Immunol.* 2: 361–367.
5. Niess, J. H., S. Brand, X. Gu, L. Landsman, S. Jung, B. A. McCormick, J. M. Vyas, M. Boes, H. L. Ploegh, J. G. Fox, et al. 2005. CX3CR1-mediated dendritic cell access to the intestinal lumen and bacterial clearance. *Science* 307: 254–258.
6. Schulz, O., E. Jaensson, E. K. Persson, X. Liu, T. Worbs, W. W. Agace, and O. Pabst. 2009. Intestinal CD103+, but not CX3CR1+, antigen sampling cells migrate in lymph and serve classical dendritic cell functions. *J. Exp. Med.* 206: 3101–3114.
7. Annacker, O., J. L. Coombes, V. Malmstrom, H. H. Uhlig, T. Bourne, B. Johansson-Lindbom, W. W. Agace, C. M. Parker, and F. Powrie. 2005. Essential role for CD103 in the T cell-mediated regulation of experimental colitis. *J. Exp. Med.* 202: 1051–1061.
8. Sun, C. M., J. A. Hall, R. B. Blank, N. Bouladoux, M. Oukka, J. R. Mora, and Y. Belkaid. 2007. Small intestine lamina propria dendritic cells promote de novo generation of Foxp3 T reg cells via retinoic acid. *J. Exp. Med.* 204: 1775–1785.
9. Jang, M. H., N. Sougawa, T. Tanaka, T. Hirata, T. Hiroi, K. Tohya, Z. Guo, E. Umemoto, Y. Ebisuno, B. G. Yang, et al. 2006. CCR7 is critically important for migration of dendritic cells in intestinal lamina propria to mesenteric lymph nodes. *J. Immunol.* 176: 803–810.
10. Coombes, J. L., K. R. Siddiqui, C. V. Arancibia-Cárcamo, J. Hall, C. M. Sun, Y. Belkaid, and F. Powrie. 2007. A functionally specialized population of mucosal CD103+ DCs induces Foxp3+ regulatory T cells via a TGF-beta and retinoic acid-dependent mechanism. *J. Exp. Med.* 204: 1757–1764.
11. Iwata, M., A. Hirakiyama, Y. Eshima, H. Kagechika, C. Kato, and S. Y. Song. 2004. Retinoic acid imprints gut-homing specificity on T cells. *Immunity* 21: 527–538.
12. Uematsu, S., K. Fujimoto, M. H. Jang, B. G. Yang, Y. J. Jung, M. Nishiyama, S. Sato, T. Tsujimura, M. Yamamoto, Y. Yokota, et al. 2008. Regulation of humoral and cellular gut immunity by lamina propria dendritic cells expressing Toll-like receptor 5. *Nat. Immunol.* 9: 769–776.
13. Uematsu, S., M. H. Jang, N. Chevrier, Z. Guo, Y. Kumagai, M. Yamamoto, H. Kato, N. Sougawa, H. Matsui, H. Kuwata, et al. 2006. Detection of pathogenic intestinal bacteria by Toll-like receptor 5 on intestinal CD11c+ lamina propria cells. *Nat. Immunol.* 7: 868–874.
14. Denning, T. L., Y. C. Wang, S. R. Patel, I. R. Williams, and B. Pulendran. 2007. Lamina propria macrophages and dendritic cells differentially induce regulatory and interleukin 17-producing T cell responses. *Nat. Immunol.* 8: 1086–1094.